Stockholm University

# Master Thesis

Degree Project in
Geochemistry 30 hp

# Estimating soluble arsenic and phosphorus concentrations under Precambrian oceanic conditions

Christoffer Hemmingsson

Stockholm 2014

Department of Geological Sciences
Stockholm University
SE-106 91 Stockholm

Acknowledgements

I would like to thank my supervisor Ernest Chi Fru for giving me the opportunity to do this project. I would also like to thank Nolwenn Callac, Nathalie Perez and Enrique Iñiguez Pacheco for much support, Jayne Rattray for much help in the lab. Beverly Chiu for her work with samples and Raman. Also regards to the help with ESEM: Marianne Ahlbom, PXRD: Henrik Skogby at NRM, BET: Zoltan Bacsik at MMK, Raman: Curt Broman for advice and running the experiment and ICP-OES: Magnus Mörth for running the analysis and going through the harsh obstacles of estimating concentrations due to analytical difficulties. This project was funded by grants from the European Research Council (Grant No: 1519901).

# Abstract

Original estimates of phosphorus (P) concentrations in the Precambrian oceans before 1.9 Ga gave a budget of ~10-25% of modern day levels. This budget was challenged by accounting for high silica (Si) concentrations that were believed to have outcompeted P for binding sites on precipitating iron oxide-hydroxide particles during the chemical oxidation and burial of iron (Fe). Such iron oxide-hydroxide particles are considered as proxies of ancient iron-rich sedimentary rocks, such as banded iron formations, which are often used to infer the dissolved chemistry of trace elements in the ancient oceans. This study raises the question of wether arsenic (As) had an effect of the binding of P to precipitating iron minerals, during the co-precipitation of Iron oxide-hydroxide in elevated Fe and Si concentrations characteristic of the early oceans. This hypothesis is based on the chemical similarities seen between P and As. Results show a more pH dependent competition between P and $As^{III}$, whereby P outcompetes $As^{III}$ at a pH <7. The effect decreases as the pH rises until pH ~8 at which the effect cancels out and $As^{III}$ becomes somewhat predominant over P. $As^{V}$ on the other hand, an analogue to P, is outcompeted by P throughout pH 5-10. Distribution coefficients (Kd) of P on iron oxide-hydroxide particles were not affected by the concentration of Si in solution. Average Kd and standard error between concentrations of Si, across the sample pH of 5-10 revealed an average Kd of 0.072 (±0.01) $\mu M^{-1}$. This is strikingly similar to another experimental Kd at 0.075 (±0.003) $\mu M^{-1}$, when the effects of Si are excluded. The average Kd in this study is also consistent with the average Kd of 0.06 $\mu M^{-1}$ from a range of As-rich hydrothermal systems reported in a previous study, supporting the original idea of Precambrian P levels being low. The average Kd between concentrations of Fe revealed a Kd of 0.12 (±0.03) $\mu M^{-1}$ although this was not statistically significant from the average Kd between groups of Si. In addition to low levels of P, the Precambrian oceans likely also contained high levels of As, due to the high hydrothermal activity. This scavenging of P from oceanic waters would have become increasingly important as surface oceans became more oxygenated and the presence of $As^{V}$ would have been greater. Because the availability of Si does not show any great effect on the uptake of P by precipitating iron oxide-hydroxides, Si concentration is likely not a proxy for oceanic P concentrations. It is proposed that low dissolved P levels are consistent with early oceans that were a lot more hydrothermally influenced than the oceans of today.



# Key Words

Arsenic, Phosphorus, Co-precipitation, Precambrian, Oceanic P levels, Ferrihydrite synthesis, Distribution coefficient, Banded iron formation.

# Sammanfattning

Prekambriska fosfor (P) nivåer var ursprungligen estimerade till ca 10-25% utav koncentrationen funnen i dagens havsvatten. Denna budget blev motsagd i och med att kisel (Si) sades kunna ersätta bundet fosfor på järn oxid-hydroxid partiklar som precipiterade genom kemisk oxidation och sedimentering av järn (Fe). Dessa järn oxid-hydroxid partiklar anses användbara som proxy för formationen av uråldriga järn-rika sedimentära bergarter såsom banded iron formation (BIF), vilka används idag för att bestämma mängden spårämnen i de uråldriga haven. Denna studie ställer frågan huruvida arsenik (As) påverkar mängden P som binder till precipiterande järn mineral under procession av co-precipitering av järn oxid-hydroxid i lösning med förhöjda koncentrationer av Fe och Si, karakteristiska för the uråldriga haven. Denna hypotes är baserad på de kemiska likheter som finns mellan P och As. Resultaten påvisar en pH beroende konkurrens mellan P och $As^{III}$ där P utkonkurrerar $As^{III}$ vid låg pH. Effekten av denna konkurrans minskar med ökande pH tills effekten blir omvänd omkring pH 8 och P blir istället till viss del utkonkurrerad av $As^{III}$. $As^{V}$ å andra sedan, en verklig kemisk analog till P, är kontinuerligt utkonkurrerad av P genom alla utförda pH, pH 5-10. Distribueringskoefficienter (Kd) för P på järn oxid-hydroxid partiklar visade ingen påverkan av mängden Si tillgängligt. Medelvärdet av Kd och standard error mellan data av alls pH, grupperat av Si, gav ett värde av 0.072 (±0.01) $\mu M^{-1}$. Detta är påfallande nära ett experimentellt framtaget Kd värde av 0.075 (±0.03) $\mu M^{-1}$ då effekten av Si är borttagen. Medelvärdet i denna studie är också sammanfallande med det Kd medelvärde man finner idag från olika hydrotemala system av 0.063 (±0.01) $\mu M^{-1}$. Detta ger support till den originala idén att de prekambriska haven troligen hade låga halter P tillgängligt. Medelvärdet av Kd mellan koncentrationer av Fe gav ett värde av 0.12 (±0.03) $\mu M^{-1}$, dock var detta värde ej statistiskt significant från det Kd utifrån koncentrationer av Si. Förutom de låga nivåer av P i de Prekambriska haven så var det troligen även höga halter av As på grund av utbredd hydrotermal aktivitet. Detta uppfångande av P i de tidiga haven var troligen en alltmer viktigare process då ytvatten blev syrerikare och den oxiderade formen av As, det vill säga $As^{V}$ hade varit mer vanligt förekommande. Framför allt då den konkurrerande effekten av Si kan bortses när P såväl som As inte påverkas av dess närvaro till den grad man hade trott. Detta gör även att mängden Si troligen inte är en tillförlitlig proxy för att estimera P nivåer i de uråldriga haven. Därmed föreslås det att de prekambriska haven var karakteriserade av låga P nivåer, jämfört med idag.

# 1.0 Introduction

Hydrothermal systems are believed to have been a common feature throughout Earth's history. The early oceans of Earth were likely dominated by ferruginous conditions demonstrated by the vast-scale deposition of banded iron formations (BIFs) (Poulton & Canfield 2011). Early earth is also believed to have had high levels of silica (Si) with hypothesised values of more than 0.67 mM and potentially as high as 2.2 mM, representing saturation with cristobalite and saturation with amorphous silica, respectively. Comparing these values in early earth to modern day levels, the modern oceans have an average of <0.10 mM Si, much less than that of early Earth (Konhauser *et al.* 2007). In addition to iron (Fe) and Si, dissolved marine phosphorus (P) concentrations through Earth's history have led to two opposing hypotheses (Bjerrum & Canfield 2002; Konhauser *et al.* 2007; Planavsky *et al.* 2010). These observations are based on comparing P concentrations preserved in BIFs to P dynamics in iron oxide-hydroxide particles precipitating in modern hydrothermal systems, by comparing scavenged P to concentrations in seawater. The first suggestion proposed low concentrations of 10-25% of present-day P levels before 1.9 Ga (Bjerrum & Canfield 2002). A subsequent study (Konhauser *et al.* 2007) instead suggested that the presence of Si reduced the amount of P preserved in BIFs, leading to underestimated dissolved seawater P values as proposed by the former authors. Konhauser *et al.* (2007) pointed out that modern hydrothermal precipitates with high Fe concentrations are not affected by Si concentrations since oceanic Si concentrations are much lower than for the Precambrian oceans. This was assumed to mean that the inferred distribution coefficient of 0.07 $\mu M^{-1}$ for the precipitates used by Bjerrum & Canfield (2002) to extrapolate their Precambrian P levels would have underestimated the impact of competing Si on dissolved P concentrations. Therefore, the Archaean ocean would have had similar P levels or even higher, compared to the oceans of today, it was concluded (Konhauser *et al.* 2007; Planavsky *et al.* 2010). Another element of importance, which has not been considered, is arsenic (As). Although the competitive uptake between P and As is known (Roberts et al. 2004) this relation has not been considered in a precambrian context. The importance of P and As lies in P being essential for life while As can be very detrimental in particular due to the similar chemistry it shares with P.

$As^{V}$ has the ability to compete with P in biological systems (Rosen *et al.* 2011). Furthermore, both elements show analogous behavioural chemistries in hydrothermal precipitates (Schaller *et al.* 2000). Due to comparable size and charge of $As^{V}$ to

phosphate, $As^{V}$ enters biological systems through phosphate transporters and obstructs the formation of ATP and nucleic acids (Bissen & Frimmel 2003; Rosen *et al.* 2011). As also competes with P uptake during the oxidation of $Fe^{II}$ to $Fe^{III}$, precipitating iron oxide-hydroxides (Schaller *et al.* 2000; Smedley & Kinniburgh 2002). Modern day sources of As are mainly associated with hydrothermal systems with important As bearing minerals primarily associated with sulphides and oxides (Smedley & Kinniburgh 2002). Hydrothermal systems are also known to have high Fe concentrations and present an ongoing process of precipitating iron oxide-hydroxides in the water column, where various anions are taken up during the formation of these iron particles (Poulton & Canfield 2006).

The early oceans likely had widespread hydrothermal activity, at least 3-4 times greater than present day (Baross & Hoffman 1985). As these systems have elevated concentrations of Fe and As and many more minor competing chemical species, the co-precipitation occurring in these systems may provide important clues into processes guiding early Earth ocean chemistry. A study of a modern hydrothermal systems revealed iron oxide-hydroxide particles retain seawater-derived P together with hydrothermally generated As, long after deposition on the seafloor (Feely *et al.* 1998; Schaller *et al.* 2000). Some P might be lost; however, most of it is retained in the sediment as primary or through secondary minerals. These observations point to the importance of iron oxide-hydroxides as a paleo-seawater proxy (Poulton & Canfield 2006).

The purpose of this study is to estimate Precambrian P and As dynamics by using ferrihydrite, an iron oxide-hydroxide, as a primary precipitate involved in the formation of banded iron formations (BIFs). The importance of ferrihydrite lies in its high surface area , sorptive capacity and competitive uptake of P, As and Si together with modelling competitive co-precipitation between P, $As^{III}$, $As^{V}$ and Si in seawater ionic strength of NaCl. The results are anticipated to provide further clues on Precambrian ocean chemistry, in particular related to dissolved P levels. Even though P co-precipitation experiments with ferrihydrite have been done previously to estimate Precambrian P-levels, simulations including P, $As^{III}$, $As^{V}$ and Si to estimate the impact of As in dissolved seawater P have never been done. This is particularly important because As strongly imposes P limitation in the modern ocean surface and directly affects primary productivity (Dyhrman & Haley 2011), and thus C burial and ocean and atmospheric oxygenation. Because P is essential for life, it has been tightly coupled with the evolution of autotrophy (Raven 2013).

## 1.1 Aims

1: This study is aimed at experimentally modelling Precambrian abiotic dissolved phosphorus concentrations during phosphorous and arsenic cycling in the process of precipitating an iron oxide-hydroxide.

2: To conduct competitive co-precipitation experiments with P and As during the oxidation of $Fe^{II}$ to precipitate an iron oxide-hydroxide. Performed in elevated iron and Si conditions thought to have been present in early Earth's oceans.

3: Re-evaluate whether Si concentrations in the early ocean conditions can indeed be used to tell oceanic P levels when in competition with stronger competitors like As for binding sites on iron oxides-hydroxides.

4: Draw conclusions of whether Precambrian oceans had high or low P and As levels.

## 1.2 Specific goals

1: To synthesise and characterise 2-line ferrihydrite under ancient oceanic conditions of elevated $Fe^{II}$ and Si in relation to P, As and Si binding.

2: To evaluate the uptake of P during the co-precipitation of such ferrihydrite particles in Fe-Si-As-rich conditions

3: Derive distribution coefficients of P from co-precipitation experiments and compare to those previously predicted for hydrothermal plumes mixing with marine P.

# 2.0 Background

## *2.1 Iron formations as a palaeo-P proxy*

The Precambrian oceans (3.8-0.524 Ga) are presumed to have been rich in Fe with the majority of the Fe originating from submarine hydrothermal systems (Poulton & Canfield 2011). The $Fe^{II}$-rich fluids when released into the water column were oxidised by biotic and abiotic processes to $Fe^{III}$ minerals that were precipitated and buried at the bottom of the ocean as BIFs (Poulton & Canfield 2011). BIFs are sedimentary deposits of alternating bands of ~20-40% Fe and ~40-50% $SiO_2$ (Konhauser *et al.* 2009). The occurrence of BIFs started at ~3.8 Ga, with recorded episodes at 3.5-2.5 Ga, 1.8 Ga and 0.8-0.6 Ga, including a maximum occurrence at 2.5 Ga (Konhauser *et al.* 2009). The stratigraphic sequences are highly variable in BIFs and the mineralogy of the least metamorphosed deposits and the mineralogy of the least metamorphosed deposits contain combinations of the minerals chert, magnetite, hematite, carbonates, greenalite, stilpnomelane, riebeckite, pyrite and minnesotaite The electron activity - hydrogen ion activity (Eh-pH) stability of these minerals and/or their precursors point predominantly towards an anoxic depositional environment (Klein 2005).

It is generally agreed that none of the major minerals in BIFs are primary minerals but rather secondary minerals formed through diagenesis and/or metamorphism with likely primary minerals being ferric hydroxide ($Fe(OH)_3$), greenalite ($(Fe)_3Si_2O_5(OH)_4$) and siderite ($FeCO_3$). Because iron oxide-hydroxides precipitate from the seawater column and settle, new layers are formed that protect the underlying layers from interacting with the water column, thus limiting trace metal mobility. Even though BIFs are considered altered to some extent, no evidence of exchange between Fe-rich layers has been seen for Archean BIFs, nor has alteration of rare earth elements (REEs) and Yttrium (Y) been observed (Konhauser *et al.* 2009).

During the deposition of BIFs, the iron oxide-hydroxide minerals would have scavenged elements such as P from the seawater column and become preserved in sedimentary memory. This ability is related to the fact that iron oxide-hydroxides such as ferrihydrite have a high surface area and high reactivity, resulting in proficient sequestration of trace elements in the depositional environment, thus recording ocean chemistry in the sediment (Poulton & Canfield 2006). The ability of iron oxide-hydroxides to precipitate and record trace element concentrations in the seawater is thus valuable in the reconstruction of oceanic nutrient and metal composition through time (Poulton &

Canfield 2006). As a consequence, BIFs are analysed to infer ocean chemistry over large geological time scales. It is particularly useful in the case of P as the fluctuations of P have been linked to variations in primary productivity and to the rise of atmospheric $O_2$ levels (Bjerrum & Canfield 2002; Konhauser *et al.* 2007; Planavsky *et al.* 2010).

A study on iron precipitates at hydrothermal vents found that dissolved oceanic P content scales proportionally with P/Fe ratios in the iron precipitates (Feely *et al.* 1998). It was shown that these iron oxide-hydroxides precipitated from the mixing of alkaline and acidic waters from hydrothermal plumes where Fe-S precipitate within seconds whereas iron oxide-hydroxides are precipitated for longer for period of time within the migrating plume. As pointed out above, the fresh precipitate reacted and scavenged several elements present in the seawater including P and As (Feely *et al.* 1998; Schaller *et al.* 2000; Poulton & Canfield 2006). It was also concluded that P and As enrichment in the iron oxide-hydroxide particles was controlled by rapid co-precipitation rather than adsorption, with the majority of enrichment occurring within the first minutes of precipitation (Schaller *et al.* 2000; Poulton & Canfield 2006).

During diagenesis, most of the iron oxide-hydroxide precipitate alters into the more stable mineral goethite and/or clays. During this process most P and As is retained in the sediment with only a small fraction of P lost (Feely *et al.*, 1998; Poulton & Canfield 2006; Schaller *et al.* 2000). This observation provided confidence that, if diagenetic processes are accounted for, P in these Fe-rich sediments can be used to estimate P budgets through geological time (Poulton & Canfield 2006). Because BIFs are thought to have developed by similar processes, they can therefore provide valuable insight into Precambrian ocean chemistry as a whole, thereby unravelling clues to the factors that limited and promoted the expansion of early life on Earth.

### *2.1.1 Ferrihydrite as a proxy of primary iron precipitates in BIFs*

The most important $Fe^{III}$ oxides (Bissen & Frimmel 2003) are $Fe^{III}$ hydroxide/ ferrihydrite ($Fe(OH)_3$), goethite (α-FeOOH), Akaganeite (β-FeOOH), Lepidocrocite (**γ**-FeOOH) and hematite ($Fe_2O_3$), with surface areas ranging from 8 to 700 $m^2/g$. Out of these minerals, ferrihydrite has the highest surface area, 100-840 $m^2/g$, of all the above mentioned minerals (Cornell & Schwertmann 2003; Weidler 1997).

Ferrihydrite has a high specific surface area (Weidler 1997) as well as a small particle size, down to nano-particles sizes of approximately ~2.6 nm (Hiemstra & Van Riemsdijk 2009). Ferrihydrite was officially recognised as a mineral in 1975. It has a poor

crystallinity (Childs 1992) seen in natural as well as synthetic samples. Ferrihydrite exists only as nano-particles and is unstable, commonly transforming into a more crystalline Fe-oxide such as goethite or hematite. The transformation of ferrihydrite can be halted or even prevented with Si in solution during precipitation (Cornell & Schwertmann 2003; Jones *et al.* 2009; Zhao *et al.* 1994).

Due to the ability of ferrihydrite to co-precipitate/adsorb high quantities of trace metals and its wide prevalence in the environment (Schwertmann & Cornell 2008), especially submarine hydrothermal fields (Feely *et al.* 1998; Schaller *et al.* 2000; Poulton & Canfield 2006), it is considered a potential precursor to several minerals found in BIFs (Klein 2005). Thus Ferrihydrite is considered one of the more important minerals that can be used to estimate palaeo-chemistry. Ferrihydrite can be synthesised as 2-line ferrihydrite and 6-line ferrihydrite, representing the most amorphous and the most crystalline forms, respectively (Cornell & Schwertmann 2003). The names 2-line and 6-line are defined by the number of peaks seen in XRD. 2-line ferrihydrite is seen as two broad bands and is the minimum number of peaks seen for ferrihydrites where two broad bands represent the most amorphous form with increasing crystallinity to 6-line, that represents the most crystalline ferrihydrite (Childs 1992). Both 2-line and 6-line ferrihydrite are prevalent in nature although 6-line ferrihydrite is typically formed in acidic conditions and high temperatures (80°C) (Schwertmann & Cornell 2008). Ferrihydrite particles have commonly been considered primary precursors for BIF deposition, though other iron minerals such as green rust can also been considered an important adsorbant for anions. Considering the wide occurrence of green rust precipitating in ferruginous conditions and the formation of green rust from ferrihydrite as well as the further transformation into magnetite (Zegeye *et al.* 2012). Even so, a large amount of work using ferrihydrite as a BIF forming iron oxide-hydroxide as model mineral has been used as inspiration for this thesis (Bjerrum & Canfield 2002; Konhauser *et al.* 2007; Planavsky *et al.* 2010; Poulton & Canfield 2011).

## *2.2 Phosphorus biogeochemical cycling*

Phosphorus (P) is one of the non-metal elements in group 15 of the periodic table, whose dissolved marine P concentrations are heavily dependent on the weathering of apatite minerals and riverine transport (Filippelli 2008). The released P is recycled and eventually ends up again as a mineral. When P reaches ocean sediments, organic P decreases during diagenesis, meanwhile authigenic P increases simultaneously (Poulton & Canfield 2006). P-rich minerals are formed during diagenesis, redistributing as well as retaining P in the sediment (Filippelli 2002).

The P cycle is also affected by large-scale events such as mountain uplift. For example the rise of the Himalayan-Tibet plateau resulted in increased weathering of P-rich minerals. This has been interpreted as a driving force in the biogenic bloom event that occurred during the late Miocene (Filippelli 2008). In addition to weathering, Filippelli (2008) suggests that glacial cycles are central to severe fluctuations in oceanic P budget because glaciers block terrestrial P sinks. A modern problem is connected to anthropogenic activity, which increases P supply to lakes, riverine input and oceanic concentrations through fertiliser application, sewage discharge, deforestation & soil loss (Fillippelli 2002).

An important P sink in the ocean comes from the scavenging activity of precipitating iron oxide-hydroxides. The precipitation of iron oxide-hydroxides causes local to area wide removal of P from the seawater column as mentioned above (Feely *et al.* 1998; Schaller *et al.* 2000; Bjerrum & Canfield 2002), affecting biological activity as a feedback (Fillippelli 2002). This would have been a common process in the suggested Fe-rich Precambrian oceans (Poulton & Canfield 2011). As a consequence, fluctuations in oceanic Fe content likely affected biological processes accordingly (Blake *et al.* 2010). BIFs are thus an important information source for reconstructing Precambrian P cycling linked to primary productivity, if subtle diagenetic processes and chemical reactions that facilitate and hinder the uptake of P by precipitating iron oxide-hydroxides are carefully taken into account. For example it has been suggested that the Iron to P ratio in BIFs can be used to backtrack dissolved P concentrations, when Si as well as other competing elements are taken into consideration (Planavsky *et al.* 2010). However, with the exemption of Si, very limited information is available on the role of even stronger P competitors such as As for binding sites on these iron precipitates.

Because Fe oxide-hydroxides particles create a P sink during co-precipitation through adsorption and incorporation, this characteristic can be expressed by a distribution coefficient defined as:

1) $[P_{ads}] = K_{ads}[P_d][Fe^{III}]$

$[P_{ads}]$ is concentration of phosphate adsorbed onto iron oxides, $[P_d]$ is concentration dissolved orthophosphate ($PO_4^{3-}$) in solution, $[Fe^{III}]$ is concentration of iron oxide particles, all concentrations are expressed in $\mu$M, and $K_{ads}$ is the adsorption constant expressed in $\mu M^{-1}$ (Bjerrum & Canfield 2002).

### *2.2.1 Phosphorus and biological activity*

P is biologically limiting for most of life in all environments on Earth, from the ocean surface to the very deep-subsurface biosphere. It is needed by both microorganisms and macroorganisms, including plants and animals (Filippelli 2002, Filippelli 2008). It is key to biological synthesis of ATP, the energy currency of the cell and for the generation of nucleic acids, the key molecules that drive the replication of the genetic code (Rosen *et al.* 2011). As a consequence, P plays an important role in processes involved in ecosystem function and biological productivity. Because P is necessary for primary productivity, the amount of dissolved P available in any ecosystem will affect its productive capacity and carbon (C) burial rates, which is all linked to the evolution of molecular oxygen by photosynthetic organisms. Thus detailed knowledge of dissolved P in the early oceans may reveal clues on the timing and rise of appreciable amounts of atmospheric oxygen some 2.5 billion years ago (Lyons *et al.* 2014).

## *2.3 Arsenic geochemistry*

Arsenic (As), one of the metalloid elements in group 15 of the periodic table, is a ubiquitous trace element (Smedley & Kinniburgh 2002). It has the following environmentally relevant oxidation states of +V, +III, 0 and –III, namely arsenate, arsenite, arsenic and arsine, respectively. As is a constituent of more than 245 minerals and is ranked as the 20$^{th}$ most abundant element in Earth's crust and is a toxic element mainly associated with iron minerals including iron oxide-hydroxides and sulphide minerals in the environment (Smedley & Kinniburgh 2002; Bissen & Frimmel 2003). $As^{III}$ is widespread in reduced environments while $As^{V}$ predominates oxygenic conditions; however, both $As^{III}$

and $As^V$ tend to co-exist in both environments but at different ratios as a function of their redox sensitivities (Smedley & Kinniburgh 2002). Most minerals associated with As are ore minerals or the alteration of these. Abundant As ore minerals are arsenopyrite (FeAsS) and arsenic-rich pyrite ($Fe(S,As)_2$). Although these sulphidic As minerals are the main association of As (Pyrite: 100-77 000 mg $kg^{-1}$ As concentration in the mineral), a strong competitor in the amount of As present in the mineral is ferrihydrite due to its high ability for As to adsorb (up to 76 000 mg $kg^{-1}$ arsenic per weight mineral). This process can create localised patches rich in As, even if an area had a low total arsenic concentration (Smedley & Kinniburgh 2002). Because of this ability of ferrihydrite (as well as other iron oxides) to bind As, the mobility of this element is dependent on the kind of adsorbing compound as well as on the pH and redox potential of the environment (Bissen & Frimmel 2003).

The model by Zeng *et al.* (2008) of individual and competitive adsorption of $As^V$ and P onto an Fe/Mn oxide with properties similar to 2-line ferrihydrite indicate a favourable adsorption of P over $As^V$. The variables used split the adsorption sites into two categories, mono-dentate (FeOH) and bi-dentate sites ($(FeOH)_2$) with the following surface acidity reactions and Log K (equilibrium constant):

1) $FeOH_2^+ = FeOH + H^+$ 6.51

2) $FeOH = FeO^- + H^+$ -9.13

In addition, the following favourable adsorption equilibrium constants are included of P over $As^V$ with the following reactions with Log K:

1) $FeOH + AsO_4^{3-} + H^+ = FeOAsO_3^{2-} + H_2O$ 16.6

2) $(FeOH)_2 + AsO_4^{3-} + 2H^+ = (FeO)_2AsO_2^- + 2H_2O$ (23.2)

3) $FeOH + PO_4^{3-} + H^+ = FeOPO_3^{2-} + H_2O$ 16.9

4) $(FeOH)_2 + PO_4^{3-} + 2H^+ = (FeO)_2PO_2^- + 2H_2O$ (23.4)

5) $FeOH_p + PO_4^{3-} + H^+ = FeO_pPO_3^{2-} + H_2O$ 16.9

6) $(FeOH_p)_2 + PO_4^{3-} + 2H^+ = (FeO_p)PO_2^- + 2H_2O$ (23.4)

### *2.3.1 Arsenic and biological activity*

In terms of biology, As is a toxic element. Organic forms are less toxic than inorganic ones with common aqueous inorganic forms found are $As^{V}$ and $As^{III}$ as weak acids and salts. For inorganic As species, $As^{III}$ is resorbed faster than $As^{V}$ in biological systems; even so, both oxidation states restrain energy-linked functions in the mitochondria, the power plant of a cell. These energy-linked functions include deactivation of enzymes by $As^{III}$ compounds as these have an affinity for sulfhydryl groups in proteins resulting in cell toxicity. $As^{V}$ competes with P in cell reactions, uncouple oxidative phosphorylation and prevents the formation of adenosine triphosphate (ATP) (Bissen & Frimmel 2003). Due to chemical similarities, As enters the cell by accident rather than because of active uptake, via phosphate transporters unable to discern between P and As (Rosen *et al.* 2011), as $As^{V}$ is chemically similar to P. $As^{III}$ behaves like glycerol at physiological pH and is taken up by aquaglycerinoporin channels (Yang *et al.* 2012). Aquaporin channels are protein channels allowing passive diffusion of water and small solutes with aquaglycerinoporin allowing glycerin in addition to water and other small solutes pass through until chemical equilibrium of concentrations is achieved (Oliva *et al.* 2010). In the aqueous environment, inorganic forms of As are found as $As^{V}$ and $As^{III}$ as weak acids and salts that can be methylated by bacteria, fungi and yeasts. The microbial methylation of arsenite ($H_3AsO_3$) and arsenate ($H_2AsO_4^-$, $HAsO_4^{2-}$) is done by replacing hydroxyl groups with methyl groups (R-CH3) forming methylarsonate ($CH_3AsO_3^{2-}$) and dimethylarsinate ($(CH_3)_2AsO_2^-$) commonly referred to as MMA and DMA respectively (Bissen & Frimmel 2003). Some microorganisms can gain energy from the oxidation of $As^{III}$ as well as reduction of AsV (Oremland & Stolz 2003); however, in many cases the reductive processes have been linked primarily to $As^{V}$ detoxification (Mukhopaghyay & Rosen 2002). Despite the redox range of As, it has not found any substantial use during electron transfer within the cell, likely due to its high toxicity.

# 3.0 Materials and methods

## *3.1 Reaction material*

Syntheses of iron oxide-hydroxide for co-precipitation reactions were made by a method based on Konhauser *et al.* (2007). The method was modified by changing the concentration of Fe and P during simultaneous addition of As to the reaction. Synthesis was carried out with the purpose of producing 2-Line ferrihydrite, as a model primary iron oxide-hydroxide mineral during the deposition of BIFs. This material was produced in solution with P, Si, $As^{III}$ and $As^{V}$ to mimic a more natural system where the precipitation of iron particles occur in the presence of a range of elements and compounds in dissolution. All experiments were performed at ambient temperature, pressure and $O_2$. The chemicals used for synthesis and reactions are presented in Table 1. Solutions were prepared as 1 M stock solutions that were diluted to the required concentration for each reaction, except for sodium chloride which was prepared at 0.56 M as all reaction were performed in solutions of 0.56 M to represent sea water ionic strength. Sample preparation of dry precipitate involved gently crushing the material in an agate mortar and pestle. For Powder X-ray diffraction (PXRD) analysis the precipitate was further crushed into a fine powder while gentle crushing was enough for Environmental Scanning Electron Microscopy using Electron dispersive spectroscopy (ESEM-EDS) and BET analysis. Synthesis of reference 2-line ferrihydrite was performed using a confirmed method by Schwertmann & Cornell (2000). Precipitation of reference ferrihydrite materials was performed by dissolving 40 g of $Fe(NO_3)_3 \cdot 9H_2O$ in MilliQ and titrating with 1 M KOH until pH 7-8 was reached, as according to the method by Schwertmann & Cornell (2000). The precipitation of reference material containing Si was performed in the presence of 0.67 mM or 2.2 mM Si in solution as suggested in the above reaction. The precipitate was then centrifuged and washed three times at ~1500-2000 rpm and air-dried in a petri dish in a laminar flow hood.

Table 1: Chemical table. Brand legend: Sigma Aldrich = SA, Merck = M, Fluka = F, Alfa Aesar = AA, Fischer Scientific = FS, Seastar = S. CAS numbers for each chemical is listed unless stated otherwise.

| Chemical name | Formula | Brand | Grade/Purity | CAS no. |
|---|---|---|---|---|
| Iron$^{II}$chloride tetrahydrate | $Cl_2Fe{\bullet}4H_2O$ | SA | >99% | 13478-10-9 |
| Iron$^{III}$nitrate nonahydrate | $Fe(NO_3)_3{\bullet}9H_2O$ | SA | ≥98% | 7782-61-9 |
| Sodium silicate solution | $Na_2O(SiO_2)x{\bullet}xH_2O$ | SA | Reagent grade | 33, 844-3 (CAT no.) |
| Potassium phosphate monobasic | $H_2KO_4P$ | F | Ultra grade, >99.5% | 7778-77-0 |
| Sodium chloride | NaCl | SA | Reagent grade | 7647-14-5 |
| Sodium hydrogen arsenate heptahydrate | $Na_2HAsO_4{\bullet}7H_2O$ | AA | 98.0-102.0% | 10048-95-0 |
| Sodium arsenite | $NaAsO_2$ | FS | Reagent grade | 7784-46-5 |
| Sodium hydroxide | NaOH | SA | Reagent grade | 1310-73-2 |
| Hydrochloric acid | HCl | S | BASELINE® grade | 7647-01-0 |
| Nitric acid | $HNO_3$ | VWR | ACS grade. Suitable for trace metal analysis. | 7697-37-2 |
| Potassium hydroxide | KOH | SA | Reagent grade, 90% | 1310-58-3 |
| Milli Q water | $H_2O$ | Q Pod system | 18.2 MQ, TOC <5 ppb | - |

## *3.2 Co-precipitation experiments*

Co-precipitation experiments were performed as replicates of 27 individual experiments, with duplicate subsamples at pH 5, 6, 7, 8, 9 and 10. The 27 experiments cover 3 concentration of iron$^{II}$ chloride (0.02, 1.0 and 2.0 mM) for each of three concentrations of Si (0, 0.67 and 2.2 mM) for each of three competitive reactions (P+As$^{III}$, P+As$^{V}$ and P+As$^{III}$+As$^{V}$). It is estimated that the early may have had dissolved FeII concentrations of 0.02 to 0.5 mM meanwhile Si concentrations are assumed to be close to cristobalite (0.67 mM) and/or near saturated amorphous Si concentrations of 2.2 mM (Bjerrum & Canfield 2002; Planavsky *et al.* 2010). In the same time, the only consensus is that both Fe and Si concentrations were higher than at present day. In this method, a scheme is used where Si to Fe ratios are assumed to fluctuate up to an ~1:1 molar ratio relative to amorphous Si. Regardless of absolute concentrations, this method allows for localised changes in Si to Fe ratios likely found between different depositional basins in the ancient oceans as well as periodically within basins as reflected by varying Si:Fe ratios

in different geographically located BIFs and within bands of the same formation (Klein 2005; Poulton & Canfield 2011). The concentrations of P and As were selected to be equimolar at 100 µM to constrain the effects of concentrations on the affinity for ferrihydrite nano-particles and does not reflect absolute concentrations. In the $P+As^{III}+As^{V}$ experiments, 50 µM of each As species was used to give a total As concentration of 100 µM. The reactions all started at pH 5, precipitating the iron as the pH was raised. Co-precipitation was performed in 250 ml volumes in sea water ionic strength 0.56 M NaCl. The solution was adjusted with HCl and NaOH to pH 5 whereby the pH was continually monitored and adjusted to remain stable for 30 min before subsamples were taken, after which pH was adjusted to pH 6, 7, 8, 9 and 10. Subsamples of 1 ml were centrifuged for ~7 minutes at ~13 000 rpm in 2 ml eppendorf tubes. After centrifuging, the supernatant was filtered through a 0.2 $\mu$m teflon filter and the remaining pellet was weighted. Both supernatant and pellet were acidified with 2 ml 5% $HNO_3$ to dissolve samples for subsequent ICP-OES analysis. Remaining solution with precipitate from co-precipitation experiments were centrifuged for ~5 min at 1500-2000 rpm. Additional supernatant was filtered and kept for storage while the remaining pellet was resuspended in a small amount of milliQ water and left to dry in a plastic petri dish for ESEM-EDS, PXRD and Raman spectroscopic analysis.

### *3.2.1. Environmental scanning electron microscopy (ESEM)*

Scanning electron microscopy (FEI, Quanta FEG 650) was used to investigate the homogeneity of samples. Sample material was prepared by gently crushing air dried precipitate in an agate mortar with pestle. The sample powder was then mounted onto aluminium stubs with carbon tape. Sample powder was not coated. Samples were investigated visually, to confirm no larger crystals had been formed, at 5 kV and low vacuum at a horizontal field view (HFW) of 1000 $\mu$m and 100 $\mu$m with images captured at different scanning speed, depending on the degree samples would charge from the excess of electrons. Samples were further investigated with energy dispersive spectroscopy (EDS) at 20 kV in low vacuum, without x-ray cone using a X-Max 80, Oxford instruments, detector. Elemental mapping was captured in the software Aztec with an averaging of 5 frames and a dwell time of 5 $\mu$s. To investigate the elemental distribution in the samples to see wether the samples have been precipitated homogeneously in terms of elemental distribution, to further confirm an amorphous iron oxide-hydroxide material has been produced.

### *3.2.2. Powder X-Ray diffraction (PXRD)*

Powder X-ray diffraction (PXRD) was obtained using a PANalytical Xpert-pro diffractometer, at room temperature. The instrument was run at 45 kV and 40 mA at 1.5406 Å wavelength using Cu-Kα radiation and Ni-filter. Samples run between 5-80° in step sizes of 0.017° and scan step time 50.1650 s in continuous scanning with rotating sample. Because of the amorphous nature of 2-line ferrihydrite, the 2 broad bands at ~34 and ~61 2θ(°) (Das & Hendry 2011), the mineral is not confirmed by the automatic reference phase detection. The confirmation of 2-line ferrihydrite is thus done visually by comparing to literature and reference spectra. The PXRD program used was 5-80° due to problems in customising running conditions. As the first 5° of the PXRD diffractogram did not yield any data of value, results are shown between 10-80°.

### *3.2.3 Specific area BET*

The surface area of materials used in adsorption experiments is important to know as it will affect the amount of adsorbed compounds. Iron oxides have varying surface areas where the poorly ordered ferrihydrite has the largest surface area between 100-840 $m^2\ g^{-1}$ (Schwertmann & Cornell 2003; Weidler 1997). As ferrihydrite dries the particles tend to form aggregates. The aggregates are commonly crushed for sample preparation of ferrihydrite for BET surface area analysis. Samples should not be exposed to water as this will cause transformation into hematite, nor exposed to acetone previous to degassing as this may decrease the surface area. The degassing of ferrihydrite is advised to be performed between 90-120°C in order to remove surface contaminants while avoiding structural transformation. Sample degassing at >120°C causes hematite and goethite to form (Weidler 1997). Schwertmann & Cornell (2000) also indicated the heating of 2-line ferrihydrite to more than 150°C transforms ferrihydrite into hematite.

The degassing procedure chosen were 50°C for 12 h. Weidler (1997) advised a temperature between 90-120°C; however, no specific time for degassing was given for these temperatures while they show that 50°C for 12 h does increase the BET surface area value given from analysis. Samples were prepared/analysed using a Micromeritics ASAP2020 volumetric adsorption analyser. Estimates of surface area were determined by calculation based on the adsorption and desorption of gas by BET, Brunauer-Emmett Theory (Brunauer *et al.* 1938). Samples were degassed in dynamic vacuum with $N_2$ at

50°C for 12 h. Adsorption-desorption isotherms were recorded while submerged in liquid nitrogen with an internal temperature of ~ -196°C. Specific surface area was then calculated according to the BET methods (Brunauer *et al.* 1938), in this case $P/P_0$ = 0.08-0.2.

### *3.2.4. Raman spectroscopy*

Raman analyses were performed with a confocal laser Raman spectrometer, Horiba instrument LabRAM HR 800, equipped with a multichannel air-cooled (-70°C) 1024*256 pixel CCD (Charge-coupled device) array detector. The instrument was coupled to a confocal Olympus BX41 microscope with laser beam focused through an 80x objective at 8 mm working distance, with resulting spot size ~1 $\mu$m. A 514 nm Argon laser (Meller Griot 543) was used as excitation source, with a laser power of 8 mW at sample surface. Spectral resolution was ~0.3 $cm^{-1}$ / pixel with instrument accuracy controlled through a silicon wafer calibration standard with a characteristic Raman line at 520.7 $cm^{-1}$. The Raman spectra were gathered using LabSpec 5.

### *3.2.5. Inductively coupled plasma optical emission spectrometry (ICP-OES)*

Elemental analysis of acidified subsamples were analysed with a Varian Vista AX, inductively coupled plasma - optical emission spectroscopy (ICP-OES) with auto sampler SPS-5. Due to the difficulty of analysing Arsenic and the high concentration of NaCl causing an interference due to ionisation of Na, concentrations of As were first underestimated. Samples were run with an external standard to correct for the ionisation of Na and adjusted by hand by Carl-Magnus Mörth, Department of geological sciences, Stockholm University. Samples run had the detection limits (in ppb) As: 5.74, Fe:1.2, P: 5.12, Si: 4.46. Sample values below detection limit has been treated as zero in the data set.

## *3.3. Software*

The graphing, treatment of data were performed using OriginPro 9.1 while SPSS statistical package V.21 was used to perform statistical analysis.

# 4.0 Results

## *4.1 ESEM*

Synthesised reference material shows an amorphous precipitate (Fig. 1). The presence of Si during precipitation did not result in any larger unwanted crystals. Elemental analysis with EDS also shows a homogenous mixture of each element (Fig. 2), indicating there are no unreacted or concentrated elements in the sample. The even distribution of Si is particularly important to ensure the Si is incorporated into the material. Colouring of elemental maps was randomly chosen by the Aztech software and is not representative of the element.

A random selection of synthesised co-precipitation samples at 100 µM horizontal field view show an amorphous precipitate with no larger crystals (Fig. 3). The appearance of cracks seen in Figure 3A and B are a result of the drying process while other size differences of grains are a result of the crushing process. EDS reveals that all elements are evenly distributed throughout the material (Fig. 4) indicating that the elements are either incorporated or adsorbed onto the Iron oxide-hydroxide particles. The appearance of shadows is a result of topography where the electron beam does not reach the sample. In the case of Figure 4C and D, there are some small areas with higher signal intensity creating an appearance of clustered elements. These areas are potentially a result of mineral transformation due to the reaction time and pH during the experiments. Average values from EDS on $As^{III}$ and $As^{V}$ samples indicate that $As^{III}$ may inhibit P uptake into the precipitating particles, while P may outcompete $As^{V}$ (Table 2). It is important to remember the samples analysed in ESEM-EDS are only from pH 10 and as such only represent high pH.

Table 2: An example of compiled EDS data from co-precipitated particles containing either $As^{III}$ or $As^{V}$, in mmol.

| | **$As^{III}$** | **$As^{V}$** |
|---|---|---|
| **Fe** | 8.1 | 9.3 |
| **O** | 30.6 | 28.8 |
| **As** | 0.61 | 0.11 |
| **P** | 0.38 | 0.37 |

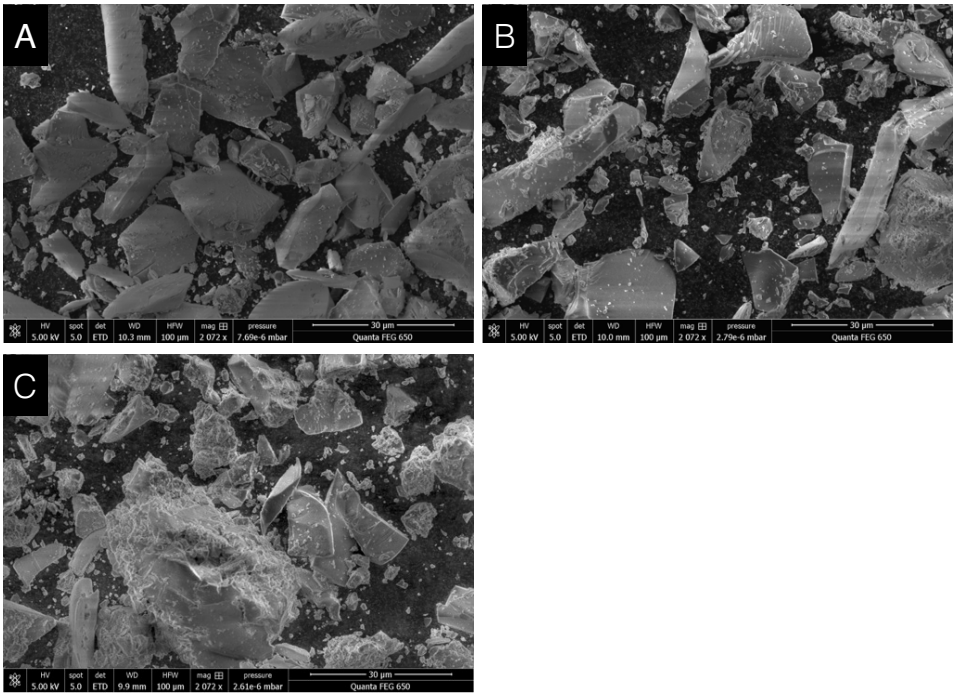


Figure 1: Iron oxide-hydroxide precipitate from the confirmed method by Schwertmann & Cornell (2000) with the addition of silica. A: 0 mM Si, B: 0.67 mM Si, C: 2.2 mM Si. With the Si/Fe ratios 0, 0.094 and 0.31, respectively.

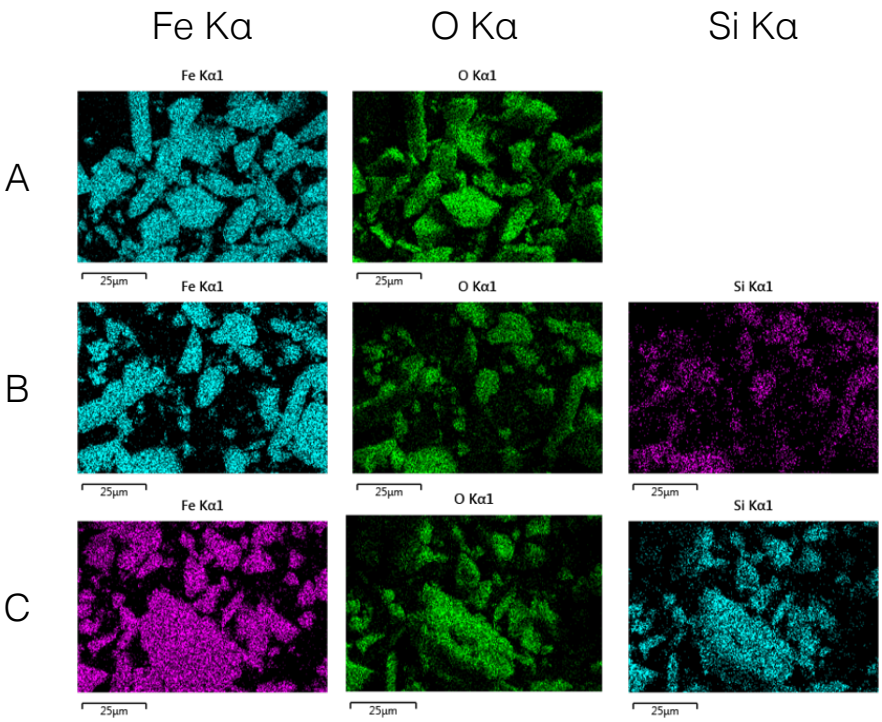


Figure 2: EDS elemental distribution maps of synthesised reference samples in three concentrations of silica. A: 0 mM Si, B: 0.67 mM Si, C: 2.2 mM Si.

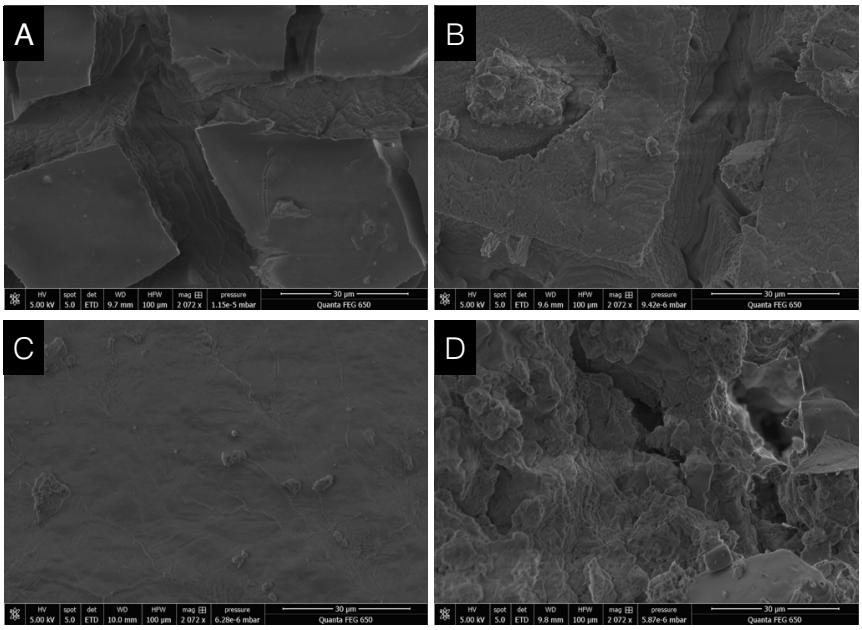


Figure 3: SEM images of Co-precipitation samples from pH 10 in low vacuum, 100 µm HFW and 5 kV. A: 1.0 mM Fe, 0 mM Si, P+As$^{III}$ B: 1.0 mM Fe, 0 mM Si, P+As$^{V}$ C: 1.0 mM Fe, 0.67 mM Si, P+As$^{III}$ D: 2.0 mM Fe, 2.2 mM Si, P+As$^{V}$.

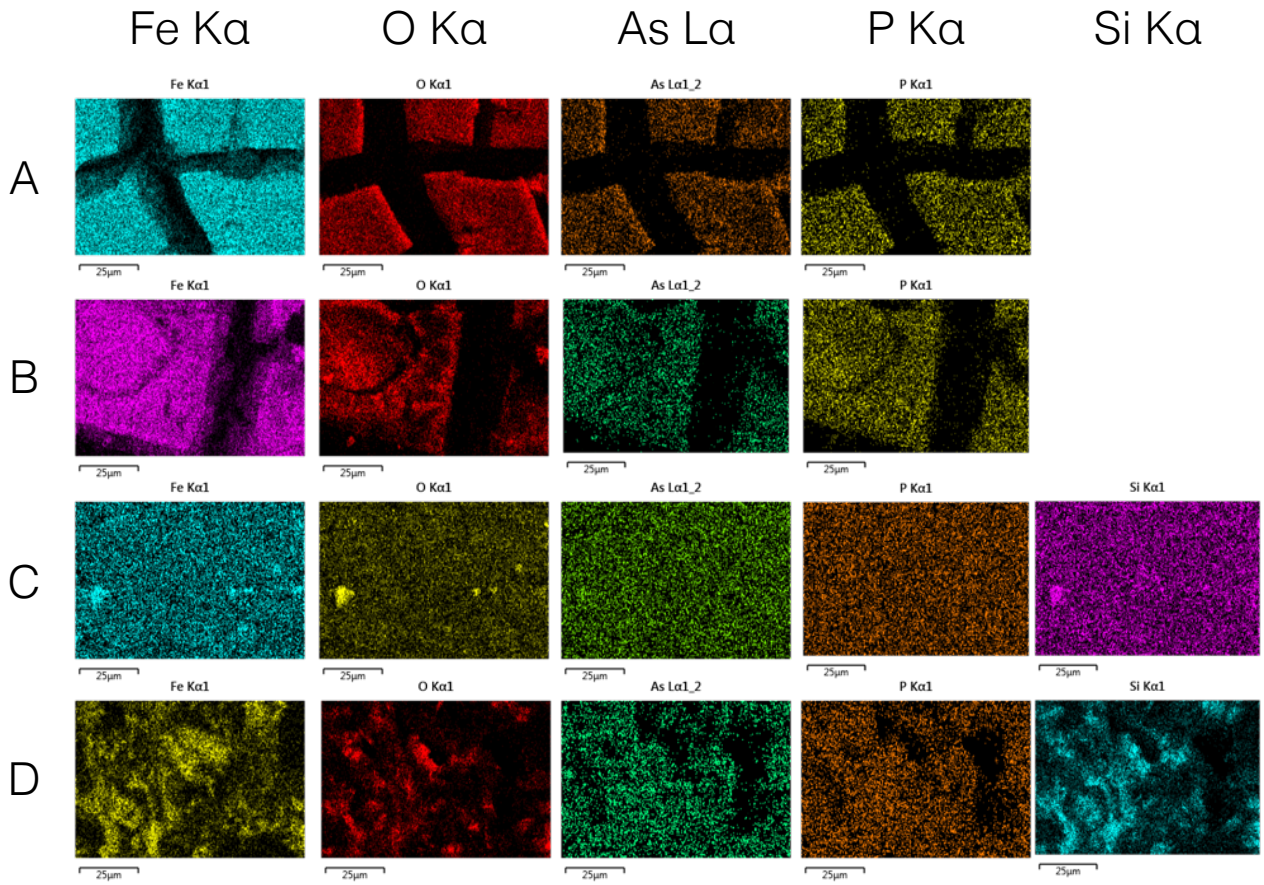


Figure 4: EDS elemental distribution of reacted samples. A: 1.0 mM Fe, 0 mM Si, P+As$^{III}$ B: 1.0 mM Fe, 0 mM Si, P+As$^{V}$ C: 1.0 mM Fe, 0.67 mM Si, P+As$^{III}$ D: 2.0 mM Fe, 2.2 mM Si, P+As$^{V}$. Na and Cl has not been included.

## *4.2 BET*

BET surface area of reference material precipitated in 0, 0.67 and 2.2 mM Si in solution show that the surface area increases with increasing Si/Fe ratio (Fig. 5). All samples show a high surface area with the smallest surface area at 331 $m^2$ $g^{-1}$ at 0 mM Si. These high surfaces areas indicate that ferrihydrite has been formed as it consists of nano-particles and thus has a high surface area due to its small size. The surface area for these samples are likely underestimated compared to the fresh precipitate, because the process of drying the material causes bonding between particles where -Fe-OH end members would likely lose $H_2O$ from -Fe-O-Fe- bonding. Thus the estimated surface areas act as a minimum surface area at best. Full list of peaks can be seen in appendix 1.

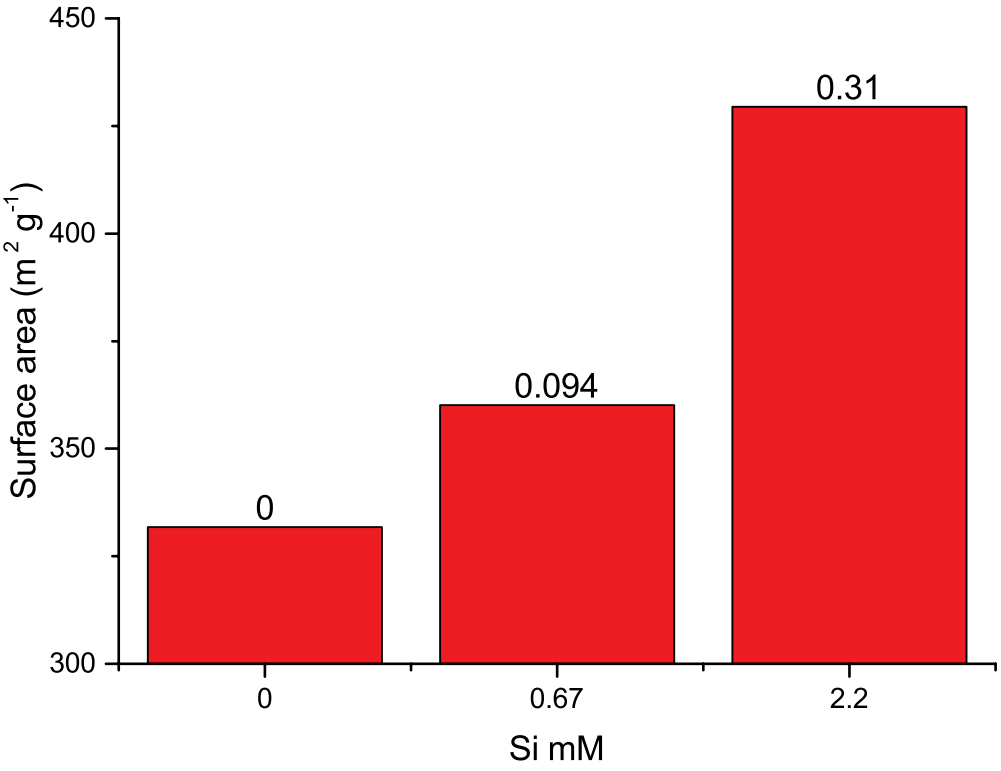


Figure 5: BET surface area of reference precipitate with Si/Fe ratio labels.

## *4.3 PXRD*

X-ray diffraction of co-precipitation particles confirm the synthesis of 2-line ferrihydrite (Fig. 6). Three samples at zero Si and with the three combinations of P and As can be seen in Figure 6. Three other samples representing three different concentrations of Si at 0, 0.67 and 2.2 mM with a single P+As combination are presented in Figure 7. Both figures show seven large peaks representing the incorporation of NaCl from solution (Fig. 6D & 7D). The same diffractogram has been displayed two times, one in black and the other in red with the red representing a zoomed in view. The red diffractogram displays the low signal as ferrihydrite is only visible this way. Ferrihydrite is seen in the two grey areas at ~36 and ~64 degrees. The samples are compared to a diffractogram of the synthesised ferrihydrite reference with 0 mM Si. The presence of ferrihydrite is more visible ~36 degrees than at 64 degrees. More importantly, the iron oxide-hydroxide produced did not yield any other more crystalline mineral phase.

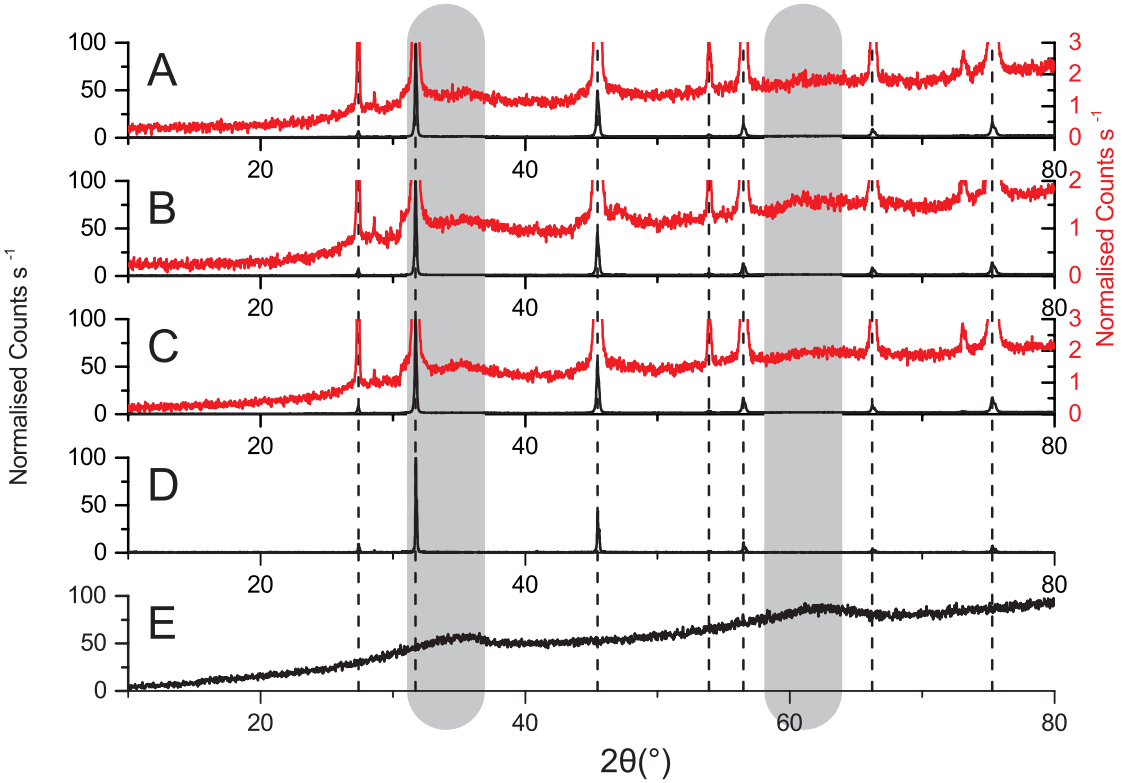


Figure 6: Normalised PXRD spectra (0-100) of samples (including Savitzky-Golay 5 point signal smoothening) and reference spectra. PXRD spectra of precipitate in 0 mM Si with different competitive sources. A: P + $As^{III}$, B: P + $As^{V}$, C: P + $As^{III}$ + $As^{V}$. D: Reference spectra of NaCl (RRUFF project. ID: R070292), E: Synthesised reference spectra of 2-line ferrihydrite by the confirmed method of Schwertmann & Cornell (2000). Dashed lines in black represent overlapping peaks with the NaCl reference. The two grey areas overlap the region where 2-line ferrihydrite typically show two broad peaks.

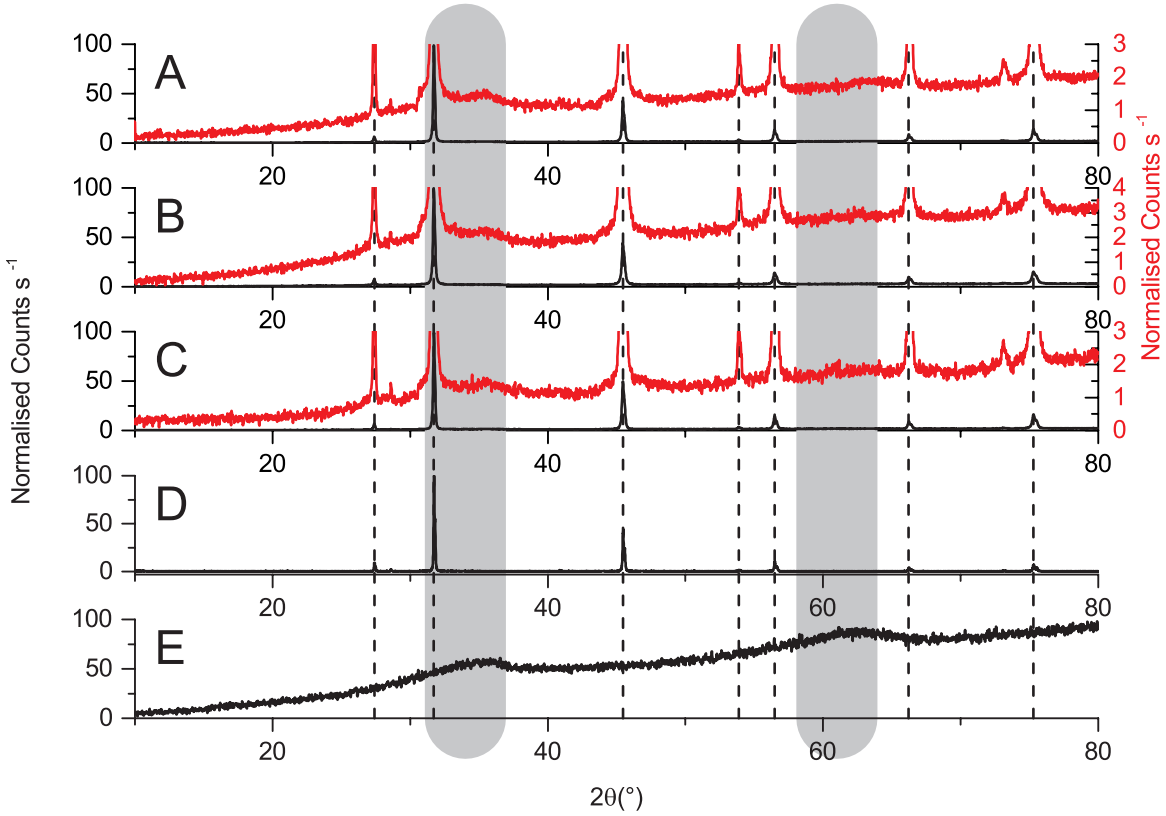


Figure 7: Normalised PXRD spectra (0-100) of samples (including Savitzky-Golay 5 point signal smoothening) and reference spectra. PXRD spectra of precipitate in P+As$^{III}$ with varying concentrations of silica. A: 0 mM Si, B: 0.67 mM Si, C: 2.2 mM Si, D: Reference spectra of NaCl (RRUFF project. ID: R070292), E: Synthesised reference spectra of 2-line ferrihydrite by the confirmed method by Schwertmann & Cornell (2000). Dashed lines in black represent overlapping peaks with the NaCl reference. The two grey areas overlap the region where 2-line ferrihydrite typically show two broad peaks.

## *4.4 Raman*

Raman scattering has revealed multiple iron oxide-hydroxide phases (not detected in ESEM-EDS & PXRD). As with PXRD, samples were investigated in a range of P+As combinations at 0 mM Si as well as three samples at different Si concentrations with a single P+As combination seen in fig 8 and 9, respectively, with a literature reference peak of synthesised ferrihydrite. As the energy used was 8 mV during analysis it is important to keep in mind that peaks can shift to a lower wavenumber as well as transform into other mineral phases. Particularly iron oxide-hydroxides are sensitive to the laser power where the transformation of a mineral can also cause the peak to shift to a higher wavenumber. Poorly crystallised minerals also cause a broadening of the peaks (Hanesch 2009). Shown in the spectra are two main phases in each sample. The phase shown in red strongly agrees with Wüstite, $Fe^{II}O$, a reduced iron oxide typically only found in high temperature environments as it is unstable below 576°C and typically form magnetite (Hazen & Jeanloz 1984). The blue coloured spectra represent the second phase in the precipitate and show a mix of mineral phases. The main phase is 2-line ferrihydrite with decomposition or transformation products of hematite and magnetite. The most important peak for 2-line ferrihydrite is at 707 $cm^{-1}$. The stronger signal of 2-line ferrihydrite is seen in samples with higher Si concentrations. This would be expected, as the oxidation of $Fe^{II}$ to form ferrihydrite is more successful in the presence of Si in solution when the molar Si/Fe ratio exceeds 0.1 meanwhile <0.1 favours precipitation of lepidocrocite (Mayer & Jarrell 1996). The presence of Si and P during the synthesis also inhibits the transformation of ferrihydrite at high pH while maintaining the amorphous nature of the mineral and inhibiting the release of P (Mayer & Jarrell 2000; Paige *et al.* 1997).

The black lines at 485, 605, 840 and 910 $cm^{-1}$ are the areas where P + $As^{V}$ adsorption is expected to be seen. There is a hint of adsorbed P present around 485 $cm^{-1}$ although this could also be masked by the presence of ferrihydrite. There is also a small peak in figure 9B around 840 $cm^{-1}$, which could be $As^{V}$. $As^{V}$ is considered to be more easily detected in Raman than $As^{III}$ due to $As^{III}$ signals being noisy and that infra red spectroscopy would be more suitable (Müller *et al.* 2010), as such the incorporation and adsorption of P and As are not easily seen in this method. Although there is more than a single mineral phase in the samples, perhaps due to pH changes as well as the amount of time exposed to liquids and during instrumental analysis the importance is the presence of ferrihydrite as shown by PXRD. The full list of Raman shift peaks can be seen in appendix 2.

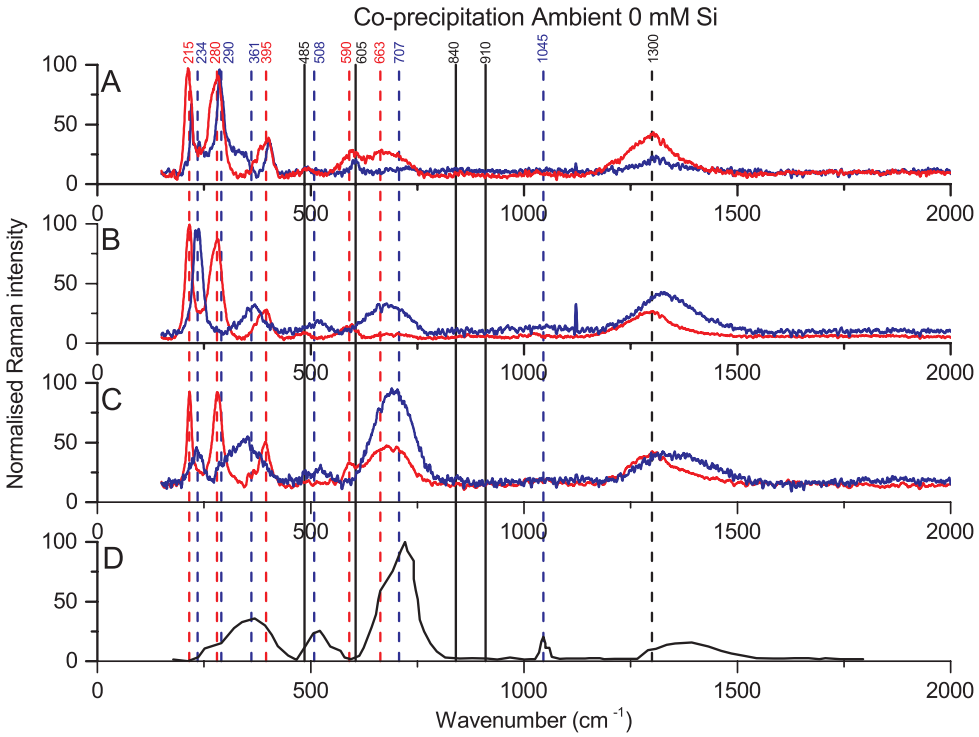


Figure 8: Baseline subtracted and normalised (0-100) Raman spectra of 3 samples in 0 mM Si with varying P+As combinations. A: P+As$^{III}$, B: P+As$^{V}$, C: P+As$^{III}$+As$^{V}$. D: Literature reference spectra of 2-line ferrihydrite (Müller *et al.* 2010).

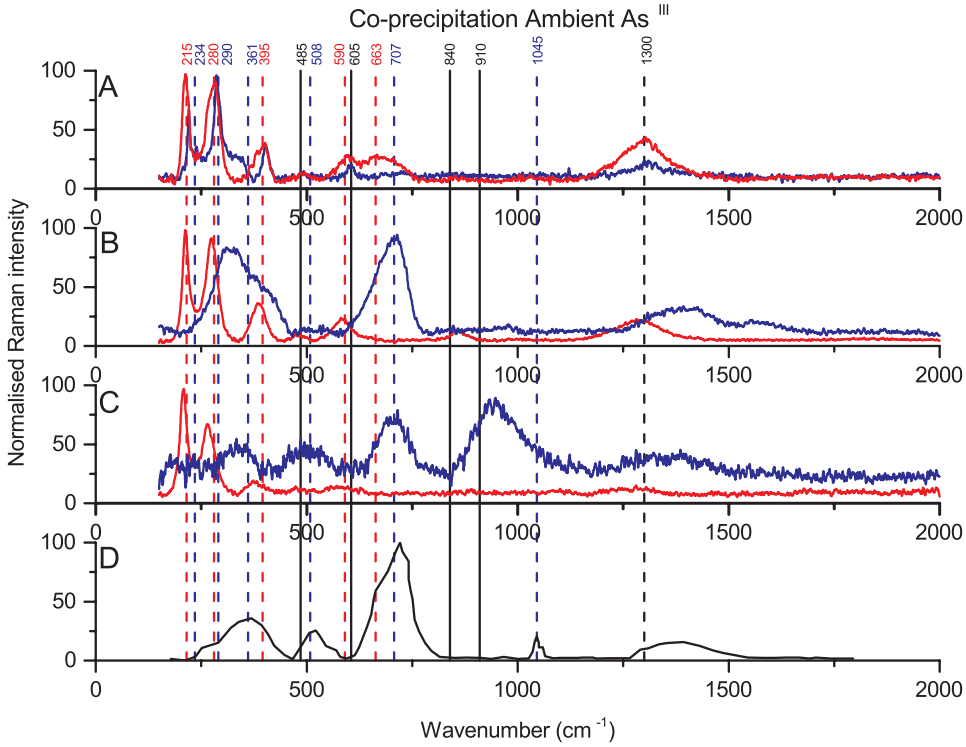


Figure 9: Baseline subtracted and normalised (0-100) Raman spectra of 3 samples in P +As$^{III}$ with varying Si concentrations. A: 0 mM Si, B: 0.67 mM Si, C: 2.2 mM Si. D: Literature reference spectra of 2-line ferrihydrite (Müller *et al.* 2010).

## *4.5 ICP-OES*

Elemental analysis revealed multiple trends dependent on pH, confirming previous trends seen in the amount of P and As present in ferrihydrite particles (Roberts *et al.* 2004). Due to the series of 0.02 mM Fe showing very noisy inconsistent patterns, this series has been excluded in the results and is focused on the 1.0 and 2.0 mM Fe series. Figure 10 and 11 show reversed trends between P and $As^{III}$ when comparing the amount of each in the solution versus the amount on the iron oxide-hydroxide particles. Showing a clear indication of the migration of P and As from the solution onto the particles. The increase of P and As around pH 6-7 is explained by the precipitation of the iron oxide-hydroxide which is typically visually confirmed around pH 6. Observing the mineral, the amount of P starts off higher than $As^{III}$ at low pH. Around pH 7-9 these concentrations cross each other resulting in higher amount of $As^{III}$ than P at high pH. The pattern repeats itself across the different Si concentrations with a small decrease in the amount of P and As on the mineral in higher Si concentration seen in figure 10. This decrease in concentration is not as clear in figure 11 with a higher iron concentration.

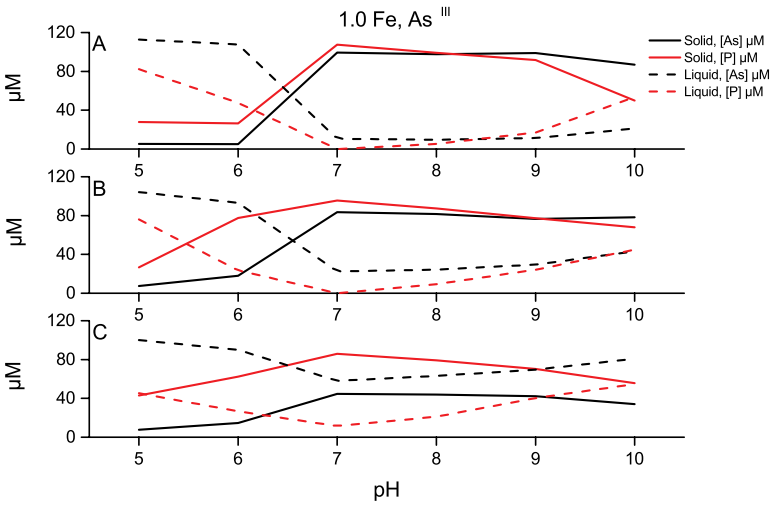


Figure 10: Elemental distribution of P and $As^{III}$ in 1.0 mM Fe subsample. Sample supernatant and precipitated pellet expressed in mol, across pH.

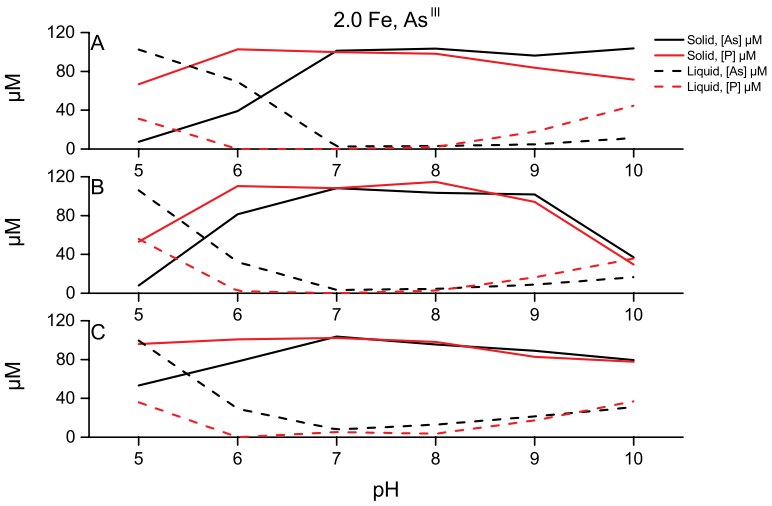


Figure 11: Elemental distribution of P and $As^{III}$ in 2.0 mM Fe subsample. Sample supernatant and precipitated pellet expressed in mol, across pH.

The $As^{V}$ experiments also reveal pH dependent trends in concentration. Figures 12 and 13 display the trends of P and $As^{V}$ in 1.0 and 2.0 mM Fe, respectively. In contrast to $As^{III}$, the concentration of P is continuously higher than $As^{V}$ on the iron oxide-hydroxide throughout the whole pH range. An anomaly seen in figure 12 and 13 is the low total concentration of As which should reach approximately 1 µmol. When comparing to EDS, the low amount of $As^{V}$ on the mineral is expected to be valid; however, the low concentration of $As^{V}$ in solution is likely an artefact from the difficulty of analysing As in ICP-OES, likely due to an ionisation effect from the high concentrations of NaCl (personal communication with Carl-Magnus Mörth, department of geological sciences, Stockholm University). This effect would not be present to the same extent in the solid phase due to the way samples have been prepared through centrifuging leaving only small amounts of NaCl in the precipitate.

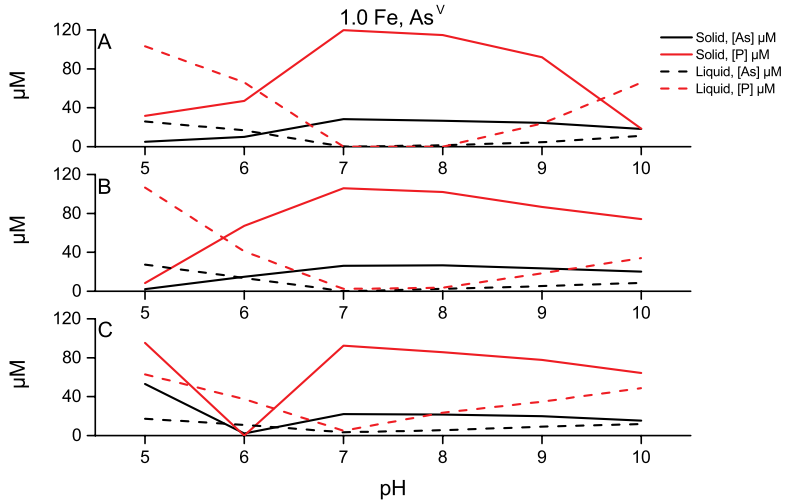


Figure 12: Elemental distribution of P and $As^{V}$ in 1.0 mM Fe subsample. Sample supernatant and precipitated pellet expressed in mol, across pH.

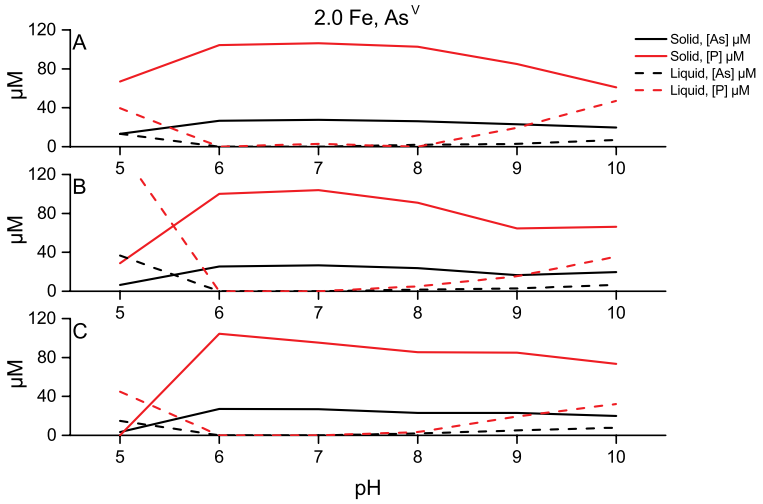


Figure 13: Elemental distribution of P and $As^{V}$ in 2.0 mM Fe subsample. Sample supernatant and precipitated pellet expressed in mol, across pH.

The samples containing combined $As^{III}$ and $As^{V}$ ($As_{tot}$) cannot have the concentrations of each valence state distinguished in ICP-OES and therefore likely displays a combination of the behaviour seen in Figures 10, 11, 12 and 13. In general the amount of P on the solid is higher than $As_{tot}$ in both 1.0 mM Fe (Fig 14) and 2.0 mM Fe (Fig 15). The amount of P is approximately the same concentration in all experiments; however, the concentration of $As_{tot}$ seen is not as high as in the $As^{III}$ experiment and not as low as in the $As^{V}$ experiment. Likely, due to half of the amount of $As^{III}$ used, the bulk of which was taken up by the mineral while $As^{V}$ mostly stayed in solution, explaining why approximately half of $As_{tot}$ is present in the mineral.

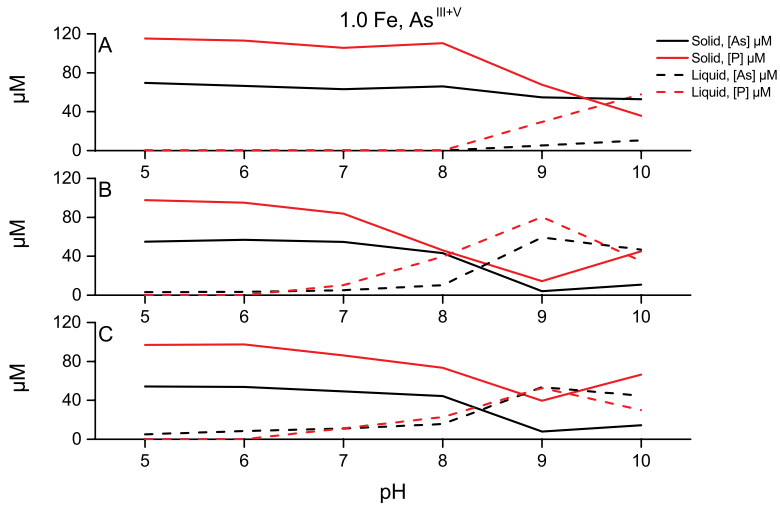


Figure 14: Elemental distribution of P and $As^{III+V}$ in 1.0 mM Fe subsample. Sample supernatant and precipitated pellet expressed in mol, across pH.

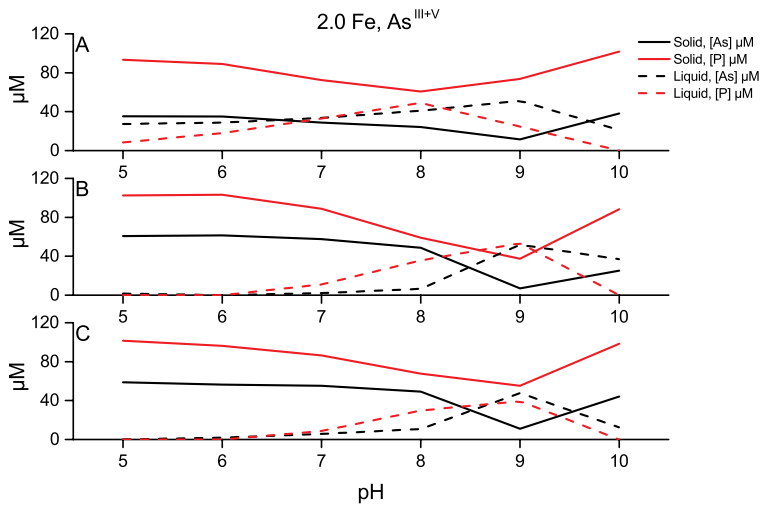


Figure 15: Elemental distribution of P and $As^{III+V}$ in 2.0 mM Fe subsample. Sample supernatant and precipitated pellet expressed in mol, across pH.

To better view the differences in $As^{III}$ and $As^{V}$ in the mineral. The As/P ratio in the mineral is displayed for 1 mM Fe in figure 16 and 2.0 mM Fe in figure 17. In figure 16 the As/P ratio increases slightly at each pH while there is a decrease when silica changes. These changes are not observed for $As^{V}$, which has a low $As^{V}$/P ratio and stays relatively constant across pH as well as across Si concentration. In figure 17 the As/P ratio also changes slightly with pH although there is not an increase with pH but rather an inconsistent change. The decrease of the $As^{III}$/P ratio with increasing silica concentration is also not seen. Indicating that the $As^{III}$/P ratio is more stable at higher iron concentrations. The $As^{V}$/P ratio for 2.0 mM Fe is low and constant as seen in figure 16. The main important pattern seen is that the competition between P and $As^{III}$ is not as strong as between P and $As^{V}$. $As^{V}$ is continuously outcompeted by P irrespective of the amount of Si present while $As^{III}$ is matched with an approximately equal amount of P on the mineral at pH 7-8.

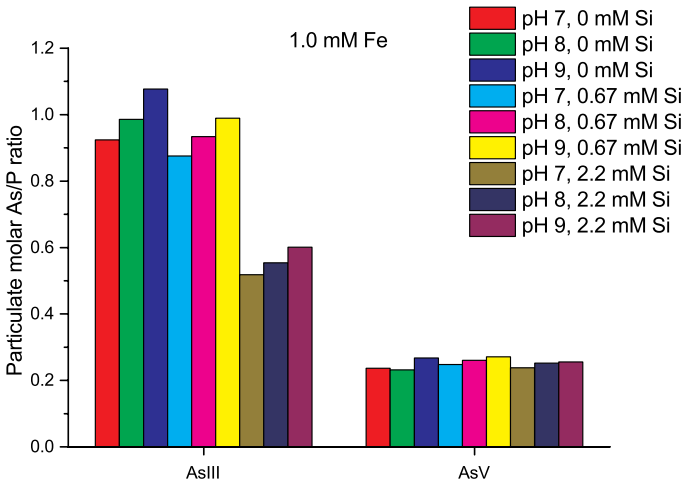


Figure 16: As/P mol ratio in subsample precipitate from $P+As^{III}$ and $P+As^{V}$ co-precipitation in 1.0 mM Fe.

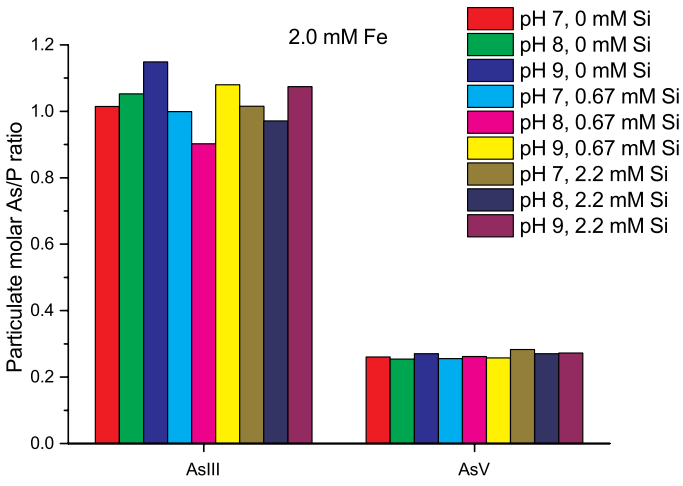


Figure 17: As/P mol ratio in subsample precipitate from $P+As^{III}$ and $P+As^{V}$ co-precipitation in 2.0 mM Fe.

Distribution coefficients of P were constructed across 1.0 and 2.0 mM Fe as well as the three Si concentrations. The distribution coefficients were made by plotting P/Fe in the iron oxide-hydroxide against P in solution for each pH. The slope that was attained was plotted with the standard error of the slope against the other samples in figure 18 for Silica and figure 19 for iron. The average Kd between Si series is 0.072 µM and 0.12 µM for the iron series. A Shapiro-wilks test of normality was run on the sample groups (Fe 1.0, 2.0 mM, Si 0, 0.67, 2.2 mM) with all groups giving $p>0.05$, meaning groups are normally distributed. A Levene's test of homogeneity of variances show homogeneity of variances between groups of Fe ($Fe=(1, 10)$ 3.774, $p>0.05$) and Si ($F=(2, 15)$ 3.306, $p>0.05$) thus retaining the null hypothesis required for analysis of variance (ANOVA). A one-way ANOVA was chosen even though sample groups are small because the assumptions have been fulfilled. The Kd showed no significant difference ($F=(2, 15)$ 0.741, $p>0.05$) between groups of Si nor between group of Iron ($F=(1, 10)$ 0.156, $p>0.05$). This means that the concentration of Si nor Fe in this study does not affect the distribution coefficient of P. There was also no significant difference seen between the two average Kd of Si and Fe ($F= (1, 28)$ 3.459, $p>0.05$).

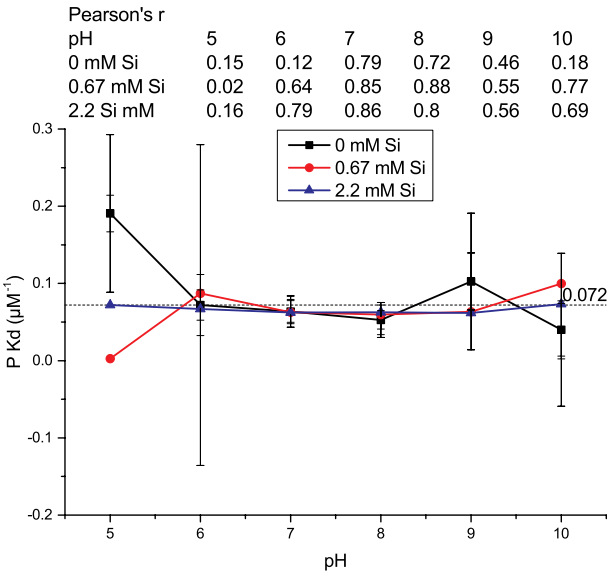


Figure 18: Phosphorus distribution coefficient (Kd) for each concentration of Si showing standard error bars. Average Kd is shown as a dotted line (0.072 ±0.01). Pearson's r of each distribution coefficient is shown on top.

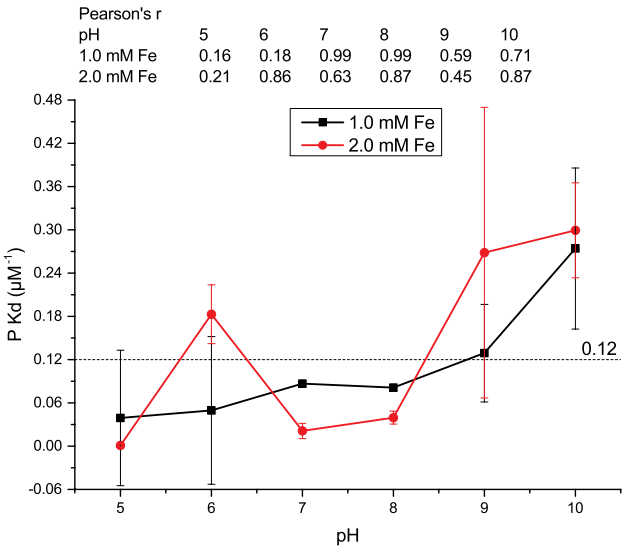


Figure 19: Phosphorus distribution coefficient (Kd) for 1.0 and 2.0 mM Fe showing standard error bars. Average Kd is shown as a dotted line (0.12 ±0.03). Pearson's r of each distribution coefficient is shown on top.

# 5.0 Discussion

The precipitation of 2-line ferrihydrite from the oxidation of $Fe^{II}$ to $Fe^{III}$ was particularly successful in the presence of Si in solution. Although, the mineral is relatively unstable, it is eventually expected to transform into more stable mineral phases such as hematite and goethite in time (Schwertmann & Cornell 2008; Schwertmann & Murad 1983; Das *et al.* 2011a; Das *et al.* 2011b). The importance of this precipitation is seen from the large amounts of P+As taken up by the mineral from solution.

The competition of P and $As^{V}$ for sites on the precipitating Fe oxide-hydroxides is of particular importance because they are chemically similar in terms of the geological as well as biological context (Bang & Meng 2004, Feely *et al.* 1998, Schaller *et al.* 2000, Smedley & Kinniburgh 2002, Elias *et al.* 2012, Rosen *et al.* 2011, Carabante *et al.* 2010). Competitive co-precipitation in ancient oxic shallow ocean conditions of high Fe and high Si (Planavsky *et al.* 2010) gives further insight into oceanic chemistry during the deposition of BIFs as ferrihydrite is traditionally used as a proxy for BIF formation (Bjerrum & Canfield 2002, Konhauser *et al.* 2007, Planavsky *et al.* 2010). There may have been other primary iron minerals involved in BIF formation such as green rust which can be formed from the reduction of ferrihydrite (Zegeye *et al.* 2012); however ferrihydrite is a primary ubiquitous iron oxide-hydroxide mineral in the environment and dominates in submarine hydrothermal precipitates (Feely *et al.* 1998; Schaller *et al.* 2000) which are believed to have been the source of BIFs (Poulton & Canfield 2011). Ferrihydrite can be easily transformed to hematite, magnetite and goethite, which are all considered secondary minerals in BIFs (Klein 2005; Konhauser *et al.* 2009). The high surface area and strong ability to incorporate and adsorb compounds from solution stress the importance of ferrihydrite in particular as a contributor to sediment chemistry. The reason that iron oxide-hydroxide rich sediments can be used as a chemistry proxy of seawater phosphorus is seen in the ability of these sediments to retain large amounts of phosphorous in the sediment (Feely *et al.* 1998; Schaller *et al.* 2000), captured by iron oxide-hydroxide precipitates (Poulton & Canfield 2006).

The average distribution coefficient of P in our experiments revealed a Kd of 0.072 (± 0.01) $\mu M^{-1}$, regardless of Si budget and pH and considering the effect of $As^{III}$ and $As^{V}$. This Kd value is very close to another experimental Kd at 0.075 (±0.003) $\mu M^{-1}$ when the effect of Si was excluded (Konhauser et al. 2007; Planavsky et al. 2010). The average Kd from a range of hydrothermal systems also gave a similar value at 0.063 (±0.01) (Feely *et al.* 1998). The average Kd when determined in relationship to changing iron concentrations

was 0.12 (± 0.03) µM-1, suggesting that fluctuations in Fe chemistry may be more important in determining dissolved P chemistry than Si.

From results in this study a simple model is suggested for the uptake of bioavailable P (orthophosphate), Arsenite ($As^{III}$) and Arsenate ($As^{V}$) from competitive co-precipitation with elevated iron in solution and seawater ionic strength of NaCl. As the data from low Fe concentrations were noisy and the increased stability of P and As retention in the precipitate with increasing Fe concentration, this points to the importance of Fe related distributions. The lack of change in the distribution coefficients of P in varying concentrations of Si can be explained by the affinity of P and As to outcompete Si during co-precipitation of iron oxide-hydroxide particles.

One explanation why Si has a limited effect on the uptake of P during the oxidation of $Fe^{II}$ to $Fe^{III}$ and in the presence of As could be the affinity of elements to adsorb onto iron oxide-hydroxide particles because co-precipitated particles include bound elements as well as adsorption of these same elements. The affinity in adsorption decreases in the order of $As^{V}$>P>$As^{III}$>Si, as determined from adsorption experiments on several iron oxide-hydroxides, including ferrihydrite (Bang & Meng 2004). This outcompeting of Si would also inhibit the lowering of the point of zero net charge (PZNC) that would otherwise prevent the adsorption of a range of elements and compounds (Konhauser *et al.* 2007). In addition to the affinity of these elements, the presence of more binding sites available for P rather than As (Zeng *et al.* 2008) likely aid in the high concentration of P. Similar to our results, competitive co-precipitation of $As^{III}$, $As^{V}$, P and Si, under non-marine conditions (Roberts *et al.* 2004), reveal that P outcompetes $As^{V}$ during the oxidation of $Fe^{II}$ to $Fe^{III}$ and show that fresh precipitate scavenges more P and As, than precipitation of iron oxide-hydroxides from a $Fe^{III}$ source with no oxidation involved. This leaves $As^{V}$ in solution while likely creating both P-limitation and acute $As^{V}$ toxicity. In similar conditions $As^{III}$ uptake is generally somewhat reduced in the presence of P and Si (Roberts et al. 2004). In the case of $As^{III}$, one needs to keep in mind that the uptake of P and $As^{III}$ is a very pH dependent reaction, as seen in this study. It is therefore suggested that the above affinity scheme may vary accordingly for $As^{V}$, $As^{III}$ and P during in situ oxidation of $Fe^{II}$ to $Fe^{III}$ and that the competitive affinity of Si for binding sites on ferric iron particles is lowered when As is present. Small variations in dissolved As and P ratios may impact bound P levels, but importantly this is not likely to enhance the effect of Si on bound P given that tested Si concentrations ranged from 0-22 times over the concentration of both As and P. In line with our results, simulations in a natural setting resulted in P being favourably bound and

removed from solution during the chemical oxidation of $Fe^{II}$ to $Fe^{III}$, while Si had a negligible effect (Roberts *et al.* 2004).

The above observations of the competitive behaviour between P and As are critical to the argument regarding elevated Precambrian oceanic silica concentrations on the early earth P budget currently extrapolated from BIFs. The interaction of dissolved marine P in Fe-As-rich natural environments (Schaller *et al.* 2000), such as the interaction of hydrothermal fluids and seawater, precipitating ferric particles, is likely complicated by the influence of a variety of minor competing chemical species. Minor competing chemical species are nonetheless disregarded in this study and due to the robust similar behaviour between P and As in both natural and simulated environmental settings (Schaller *et al.* 2000; Roberts *et al.* 2004), our data strongly indicate that the amount of P bound and removed from solution by precipitating iron particles is likely more linked to the dissolved As/P ratio than to competing chemical species with less affinity such as Si. Furthermore, due to the chemical similarity between P and As, the diagenetic behaviour of P and As reflect one another (Edenborn *et al.* 1986; Schaller *et al.* 2000; Poulton & Canfield 2006). The burial of P and As in submarine Fe-As-rich hydrothermal systems is controlled mainly by rapid co-precipitation rather than plain adsorption reactions with ferric iron oxide-hydroxide particles (Feely *et al.* 1998; Schaller *et al.* 2000). This is based on the observation that the concentration of both elements in these particles stay relatively constant during long distance transportation (Feely *et al.* 1998; Schaller *et al.* 2000). The retained P and As appear to be partially released from the ferric particles by diagenetic processes such as recrystallisation and reductive $Fe^{III}$ dissolution. The total amount of P and As covaries with the concentration of Fe in the sediment (Feely *et al.* 1998; Schaller *et al.* 2000). The released fraction which does not recrystallise nor adsorb in the sedimentary pore water are further re-precipitated at the water sediment-surface interface (Poulton & Canfield 2006).

A low P budget of the early earth oceans, compared to present day levels, was first predicted by using a Kd similar to the one found in this study (Bjerrum & Canfield 2002). This resulted in the suggestion that after ~2.5 Ga when the atmospheric $O_2$ levels increased from virtually zero to present-day levels (Lyons *et al.* 2014) the dissolved oceanic P level dropped by almost one magnitude. Dissolved phosphorus levels were estimated at pre-2.5 Ga levels of 0.11-0.29 μM to post-2.5 Ga levels of 0.03-0.09 μM (Bjerrum *et al.* 2002). A minimum of 0.04 μM with confirmed standard deviation of 0.03 was recorded ~2.0 Ga, after which atmospheric $O_2$ levels are believed to have dropped to

pre-2.5 Ga levels. This potential lowering of oceanic phosphate levels may be due to a higher biological demand for phosphate by extant organisms in the oxygenated surface ocean (Lyons *et al.* 2014). The increased atmospheric availability of $O_2$ at ~2.5 Ga also oxygenating the ocean may have increased the loss of P from oceanic waters into the sediment from an increased precipitation of iron oxide-hydroxides. An increase of P sequestration would in turn leave dissolved $As^{V}$ and further affect primary productivity. The available P and As, in sufficient concentration, would have outcompeted Si for binding sites on iron oxide-hydroxide minerals, preventing the lowering of the PZNC and allowing particles to further scavenge P in solution, in contrary to the previous hypothesis of Si playing an important role as a proxy for P concentrations. High Si concentrations affect the precipitation of ferrihydrite by increasing the surface area and create smaller particle size with increased Si concentrations during precipitation. The higher surface area may scavenge higher concentrations of P through a process of substitution, not investigated in this study but seen in the $As^{III}$/P ratio where an increased amount of P remains in solution at 1.0 mM Fe. This pattern is then removed when Fe is increased to 2.0 mM. One may speculate that periods of P shortage and As toxicity in the early ocean could have resulted in the development of As resistance and detoxification by reducing $As^{V}$ to $As^{III}$ meanwhile favouring high affinity of P in metabolic pathways, aiding cyanobacteria to survive (Dyhrman & Haley 2011).

# 6.0 Conclusions

This study indicates that the effect of Si is strongly reduced by competitive co-precipitation of an iron oxide-hydroxide in the presence of P and As. $As^{III}$ and P compete to some degree which is particularly related to pH with P outcompeting $As^{III}$ at low pH while $As^{III}$ outcompetes P at high pH and with a cancelled effect around pH 7-9 at which P and $As^{III}$ cross paths. $As^{V}$ on the other hand is continuously outcompeted by P and would be the main process expected in oxidised conditions. The distribution coefficient of P is not affected by silica, likely due to the competition of attachment sites on ferrihydrite. These processes could be combined with the formation of BIF as a proxy of seawater chemistry on at least local scales with frequent precipitation of iron oxide-hydroxide. The low $As^{V}$/P ratio on the iron oxide-hydroxide particles indicate that Precambrian oceans dealt with low soluble P and high As concentrations from time to time, likely affecting primary productivity.

This study suggests that oceanic dissolved P levels linked to primary productivity in the Precambrian oceans have varied greatly due to the effects of hydrothermal activity in ocean basins, As and $Fe^{II}$ concentrations, distances from volcanic area/hydrothermal areas and soluble P levels. Regarding hydrothermal systems, Si likely had little to no effect in the scavenging of elements with higher affinity for iron oxide-hydroxides, contrary to current thoughts. The low dissolved P budget of early oceans likely prevented the growth of primary productivity, seen as reduced carbon burial rates and as a consequence affected the oxygen production and accumulation in Earth's early geobiosphere, particularly after the large increase in atmospheric $O_2$ levels after 2.5 Gyr.

# 7.0 References

Bang S. & Meng X. (2004) A review of arsenic interactions with anions and iron hydroxides. Environmental engineering research. 9: 184-192.

Baross J.A. & Hoffman S.E. (1985) Submarine hydrothermal vents and associated gradient environments as sites for the origin and evolution of life. Origins of life. 15: 327-345.

Bissen M. & Frimmel F.H. (2003) Arsenic - A review: Part I: Occurrence, toxicity, speciation, mobility. Acta hydrochimica et hydrobiologica. 31 (1): 9-18.

Bjerrum C.J. & Canfield D.E. (2002) Ocean productivity before about 1.9 Gyr ago limited by phosphorous adsorption onto iron oxides. Nature 417:159-162. + SI.

Blake R.E., Jung Chang S. & Lepland A. (2010) Phosphate oxygen isotopic evidence for a temperate and biologically active Archaean ocean. Nature, Letters. 464: 1029-1032.

Brunauer S., Emmett P.H. & Teller E. (1938) Adsorption of gases in multi molecular layers. Journal of the American chemical society. 60: 309-319.

Carabante I., Grahn M., Holmgren A. and Hedlund (2010) In situ ATR-FTIR studies on the competitive adsorption of arsenate and phosphate on ferrihydrite. Journal of colloid and interface science. 351 (2): 523-531.

Childs C.W. (1992) Ferrihydrite: A review of structure, properties and occurrence in relation to soils. Z. Pflanzenernähr. Bodenk. 155: 441-448.

Cornell R.M. & Schwertmann U. (2003) The iron oxides: Structure, properties, reactions, occurrences and uses. 2nd Ed. Wiley-VCH Verlag GmbH & Co. KGaA, Weinheim.

Das, S. & Hendry M.J. (2011) Application of Raman spectroscopy to identify iron minerals commonly found in mine wastes. Chemical geology. 290: 101-108.

Das S., Hendry M.J. & Essilfie-Dughan J. (2011a) Effects of adsorbed arsenate on the rate of transformation of 2-line ferrihydrite at pH 10. Environmental science and technology. 45: 5557-5563.

Das S., Hendry M.J. & Essilfie-Dughan J. (2011b) Transformation of two-line ferrihydrite to goethite and hematite as a function of pH and temperature. Environmental science and technology. 45: 268-275.

Edenborn H.M., Belzile N., Mucci A., Lebel J. & Silverberg N. (1986) Observations on the diagenetic behaviour of arsenic in a deep coastal sediment. Biogeochemistry. 2: 359-376.

de Faria D.L.A. & Lopes F.N. (2007) Heated goethite and natural hematite; Can Raman spectroscopy be used to differentiate them?. Vibrational spectroscopy. 45: 117-121.

de Faria D.L.A., Venâncio Silva, S. & de Oliveira M.T. (1997) Raman microspectroscopy of some iron oxides and oxyhydroxides. Journal of raman spectroscopy. 28: 873-878.

Dyhrman, S. T. & Haley, S. T. (2011) Arsenate resistance in the unicellular marine diazotroph *Crocosphaera Watsonii.* Frontiers in Microbiology. 2: 214

Elias M., Wellner A., Goldin-Azulay K., Chabriere E., Vorholt J.A., Erb T.J. & Tawfik D.S. (2012) The molecular basis of phosphate discrimination in arsenate-rich environments. Nature. 491 (7422): 134-137.

Feely R.A., Trefry J.H, Lebon G.T. & German C.R. (1998) The relationship between P/Fe and V/Fe ratios in hydrothermal precipitates and dissolved phosphate in seawater. Geophysical research letters. 25 (13): 2253-2256.

Filippelli G.M. (2002) The global phosphorus cycle. Reviews in mineralogy and geochemistry. 48 (1): 391-425.

Filippelli G.M. (2008) The global phosphorus cycle: past, present, and future. Elements 6: 89-95.

Hanesch M. (2009) Raman spectroscopy of iron oxides and (oxy)hydroxides at low laser power and possible applications in environmental magnetic studies. Geophysical journal international. 177: 941-948.

Hazen R.M. & Jeanloz R. (1984) Wüstite (Fe1-xO): A review of its defect structure and physical properties. Reviews of geophysics and space physics. 22 (1): 37-46.

Hiemstra T. & Van Riemsdijk W.H. (2009) A surface structural model for ferrihydrite I: Sites related to primary charge, molar mass, and mass density. Geochimica et cosmochimica acta. 73: 4423-4436.

Jia, Y., Xu, L., Fang, Z. & Demopoulos G.P. (2006) Observation of surface precipitation of arsenate on ferrihydrite. Environmental science and technology. 40: 3248-3253.

Jones A.M., Collins N.R., Rose J. and Waite T.D. (2009) The effect of silica and natural organic matter on the Fe(II)-catalysed transformation and reactivity of Fe(III) minerals. Geochimica et cosmochimica acts. 73: 4409-4422.

Kawazoe, H., Yanagita, H., Watanabe, Y., & Yamane, M. (1988). Imperfections in amorphous chalcogenides. I. Electrically neutral defects in liquid sulfur and arsenic sulfides. Physical Review B. 38 (8): 5661-5667.

Klein C. (2005) Some Precambrian banded iron-formations (BIFs) from around the world: Their age, geologic setting, mineralogy, metamorphism geochemistry, and origin. American mineralogist. 90: 1473-1499.

Konhauser K.O., Lalonde S.V., Amskold L. & Holland H.D.h (2007) Was there really an Archaean phosphate crisis. Science 315:1234.

Konhauser K.O., Pecoits E., Lalonde S.V., Papineau D., Nisbet E.G., Barley M.E., Arndt N.T., Zahnle K. & Kamber B.S. (2009) Oceanic nickel depletion and a methanogenic famine before the great oxidation event. Nature. 458: 750-753. + SI.

Lyons T. W., Reinhard C. T. & Planavsky N. J. (2014) The rise of oxygen in Earth's early ocean and atmosphere. *Nature.* 506: 307–315.

Mayer T.D. & Jarrell W.M. (1996) Formation and stability of f iron(II) oxidation products under natural concentrations of dissolved silica. Water research. 30 (5): 1208-214.

Mayer T.D. & Jarrell W.M. (2000) Phosphorus sorption during iron(II) oxidation in the presence of of dissolved silica. Water research. 34 (16): 3949-3956.

Mazzetti L. & Thistlethwaite P.J. (2002) Raman spectra and thermal transformations of ferrihydrite and schwertmannite. Journal of raman spectroscopy. 33: 104-111.

Mukhopadhyay R. & Rosen B.P. (2002) Arsenate reductases in prokaryotes and eukaryotes. Environmental Health And Perspectives. 110 (S5): 745-748.

Müller K., Ciminelli V.S.T., Dantas M.S.S. & Willscher S. (2010) A comparative study of As(III) and As(V) in aqueous solutions and adsorbed on iron oxy-hydroxides by Raman spectroscopy. Water research. 44: 5660-5672.

Oliva R., Calamita G., Thornton J.M. & Pellegrini-Calace M. (2010) Electrostatics of aquaporin and aquaglyceroporin channels correlates with their transport selectivity. PNAS. 107 (9): 4135-4140.

Oremland R.S & Stolz J.F. (2003) The ecology of arsenic. Science. 300 (5621): 939-944.

Paige C.R., Snodgrass W.J., Nicholsin R.V., Scharer J.M. & He Q.H. (1997) The effect of phosphate on the transformation of ferrihydrte into crystalline products in alkaline media. Water, Air, and soil pollution. 97: 397-412.

Paktunc D., Dutrizac J. & Gertsman V. (2008) Synthesis and phase transformations involving scorodite, ferric arsenate and arsenical ferrihydrite: implications for arsenic mobility. Geochimica et cosmochimica acta. 72: 2649-2672.

Planavsky N.J., Rouxel O.J., Bekker A., Lalonde S.V., Konhauser K.O., Reinhard C.T. & Lyons T.W. (2010) The evolution of the marine phosphate reservoir. Nature 467:1088-1090.

Poulton S.W. & Canfield D.E. (2006) Co-diagenesis of iron and phosphorus in hydrothermal sediments from the southern East Pacific Rise: Implications for the evaluation of paleoseawater phosphate concentrations. Geochimica et cosmochimica acta. 70: 5883-5898.

Poulton S.W. & Canfield D.E. (2011) Ferruginous conditions: a dominant feature of the ocean through Earth's history. Elements. 7: 107-112.

Raven J.A. (2013) Th evolution of autotrophy in relation to phosphorus requirement. Journal or experimental botany. 64 (13): 4023-4046.

Roberts L.C., Hug S.J., Ruettimann T., Morsaline Billah M.D. Wahab Khan A. & Tariqur Rahman M. (2004) Arsenic removal with Iron(II) and Iron(III) in waters with high silicate and phosphate concentrations. Environmental science and technology. 38: 307-315.

Rosen B.P., Ajees A.A. & McDermott T.R. (2011) Life and death with arsenic. Bioessays. 33: 350-357.

RRUFF project. ID: R070292. Halite. http://rruff.info/halite/display=default/R070292. Peak list: http://rruff.info/repository/sample_child_record_powder/by_minerals/Halite__R070292-1__Powder__Cell_Refinement_Data__8527.txt. Retrieved 2014-06-13.

Schaller T., Morford J., Emerson S.R. & Feely R.A. (2000) Oxyanions in metalliferous sediments: Tracers for paleoseawater metal concentrations?. Geochimica et cosmochimica acta. 63 (13): 2243-2254.

Schwertmann U. & Cornell R.M. (2008) Iron oxides in the laboratory: preparation and characterization. Second, Completely revised and extended edition. Wiley-VCH Verlag GmbH.

Schwertmann U. & Murad E. (1983) Effect of pH on the formation of goethite and hematite from ferrihydrite. Clays and clay minerals. 31 (4): 277-284.

Shebanova O.N. & Lazor P. (2003) Raman spectroscopic study of magnetite ($FeFe_2O_4$): a new assignment for the vibrational spectrum. Journal of solid state chemistry. 174 (2): 424-430.

Smedley P.L. & Kinniburgh D.G. (2002) Review: A review of the source, behaviour and distribution of arsenic in natural waters. Applied geochemistry. 17: 517-568.

Thibeau R.J., Brown C.W. & Heidersbach R.H. (1978) Raman spectra of possible corrosion products of iron. Applied spectroscopy. 32 (6): 532-535.

Weidler P.G. (1997) BET sample pretreatment of synthetic ferrihydrite and its influence on the determination of surface area and porosity. Journal of porous materials. 4: 165-169.
Yang H.C., Fu H.L., Lin Y.F., and Rosen B.P. (2012) Pathways of arsenic uptake and efflux. In: Current topics in membranes. Ed. Lutsenko S. & Arguello J.M. Vol. 69: 325-358.

Zaghib, K., & Julien, C. (2005). Structure and electrochemistry of $FePO_4 \cdot 2H_2O$ hydrate. Journal of Power Sources, 279-284.

Zegeye A., Bonneville S., Benning L.G., Sturm A., Fowle D.A., Jones C., Canfield D.E., Ruby C., MacLean L.C., Nomosatryo S., Crowe S.A. & Poulton S.W. (2012) Green rust formation controls nutrient availability in a ferruginous water column. Geology. 40 (7): 599-602.

Zeng H., Fisher B. & Giammar D.E. (2008) Individual and competitive adsorption of arsenate and phosphate to a high-surface-area Iron Oxide-based sorbent. Environmental science and technology. 42: 147-152.

Zhao J., Huggins F.E., Feng Z. and Huffman G.P. (1994) Ferrihydrite: surface structure and its effects on phase transformation. Clays and clay minerals. 42 (6): 737-746.

# Appendix

## *Appendix 1*

List of PXRD peaks and references.

| 2θ(°) | Mineral | Ref |
|---|---|---|
| 27.4 | Halite | RRUFF project. ID: R070292 |
| 31.7 | Halite | RRUFF project. ID: R070292 |
| 34 (Broad peak) | Ferrihydrite | Das & Hendry 2011 |
| 45.47 | Halite | RRUFF project. ID: R070292 |
| 53.89 | Halite | RRUFF project. ID: R070292 |
| 56.49 | Halite | RRUFF project. ID: R070292 |
| 61 (Broad peak) | Ferrihydrite | Das & Hendry 2011 |
| 66.24 | Halite | RRUFF project. ID: R070292 |
| 75.31 | Halite | RRUFF project. ID: R070292 |

# *Appendix 2*

List of peaks in Raman spectroscopy and references.

| **Wavenumber ($cm^{-1}$)** | **Mineral / Phase / Sorption** | **Reference** |
|---|---|---|
| 215 | Wüstite | de Faria *et al.* 1997 |
| 230 | As-As homopolar bond | Kawazoe *et al.* 1988 |
| 230-235 | Hematite | de Faria *et al.* 1997; Das & Hendry 2011 |
| 270-280 | Wüstite | de Faria *et al.* 1997 |
| 290 | Magnetite | de Faria *et al.* 1997 |
| 358-361 | Ferrihydrite | Müller *et al.* 2010; Das & Hendry 2011 |
| 390-395 | Wüstite | de Faria *et al.* 1997 |
| 480-485 | v2 PO43 | Zaghib & Julien 2004 |
| 508 | 2-line Ferrihydrite | Das & Hendry 2011 |
| 590 | Wustite | de Faria *et al.* 1997 |
| 605 | v4 PO43 | Zaghib & Julien 2004 |
| 663-667 | FeO and Magnetite from FeO transformation; Magnetite peak | de Faria *et al.* 1997; Thibeau *et al.* 1978; Müller *et al.* 2010 |
| **707** | 2-line Ferrihydrite | Das & Hendry 2011 |
| 836-840 | Adsorbed AsV | Das & Hendry 2011; Müller *et al.* 2010 |
| 910 | As+V Sorption | Jia *et al.* 2006 |
| 1045 | 2-line Ferrihydrite | Das & Hendry 2011 |